Journal of Nepal Geological Society, 2020, vol. 60, pp. 1-20
https://doi.org/10.3126/jngs.v60i0.31272

Geochemical signatures of recent bar deposits in the Tista river, Bangladesh: Implications to provenance, paleoweathering and tectonics

***Pradip Kumar Biswas[1,2], M. Shafiqul Alam[2], A.S.M. Mehedi Hasan[1], Syed Samsuddin Ahmed[2], Mohammad Nazim Zaman[1]**

[1]Institute of Mining, Mineralogy and Metallurgy (IMMM), Bangladesh Council of Scientific and Industrial Research (BCSIR), Joypurhat, Bangladesh
[2]Department of Geology and Mining, University of Rajshahi, Rajshahi, Bangladesh
**Corresponding author's email:pradip_immm@yahoo.com*

ABSTRACT

Petrography and geochemical composition of sediments is a sensitive indicator which archives the signature of a previous record of a source rock and depositional environments in a basin. This study deals with the elemental geochemistry of recent bar deposits of the Tista river in the north western part of Bangladesh to evaluate their provenance, paleoweathering and tectonic setting. Petrographically, the sediments are rich in quartz (70%), whereas feldspar and lithic fragments are found about 8% and 3%, respectively. The geochemical composition of the samples exhibits dominantly quartzose litharenites with low grade sedimentary and metasedimentary lithics, low feldspar indicates tectonic provenance field of recycled orogeny. Discrimination functions revels that the sediments of the Tista river are the derivation of active continental margin. The analyses also reflect that the sediments are dominantly a mixture of felsic (e.g., granitic/Gneiss, quartzite, amphibolite, granulite facies rock types) and some of mafic source (e.g., alkali-basalt/greenschist facies). It may occur, since 60% of the sedimentary flux carried out by the river from low-grade metamorphic rock and the rest from high-grade rock (in the west and north Sikkim Himalaya respectively). The weathering indices highlight that the source rocks have not undergone significant chemical weathering. The immature sorting status and petrographic evidences indicate that the sediments deposited in the Tista river basin are simply the product of mechanically weathered rocks.

Keywords: Geochemistry; Tista river; Provenance; Paleoweathering; Principal component analysis; Bangladesh

Received: 9 June, 2020 **Received in revised form:** 10 July, 2020 **Accepted:** 22 August, 2020

INTRODUCTION

The petrography and geochemistry of clastic sediments represent an archive for understanding of sand provenance, the tectonics as well as weathering conditions of the source (Cullers, 2000; Kumar et al., 2019; Noa Tang et al., 2020). The bulk compositions of sediments- major elements, trace elements, rare earth elements (REEs) and their elemental ratios are the sensitive indicators which reserve the signs involving of these processes from source to basin. This allows examining the role of these factors and simultaneously unraveling the record of past sedimentary environments in the Bengal Basin, a deepest sedimentary basin of the world (Curray and Moore, 1971; Roy and Roser, 2013). Accordingly, geochemical and petrographical analyses (Garzanti et al. 2020) of the Tista river basin sediments in the north western part of Bangladesh is an ideal location to observe the tectonic uplift and erosion history of the Himalaya and also paleoweathering.

The Tista river is one of the main Himalayan tributaries of the Brahmaputra river, originated from glaciers in the North Sikkim, flows over the northern part of Bangladesh (Fig. 1). The river drains sediments from most of the Himalayan tectonic units towards the southwest into the Rangit river at Triveni territory (Fig. 1a). The sedimentary flux of Tista catchment, amounting to around 4×10^6 ton/year and approximately 60% of the total Tista sand flux in Bangladesh comes from the Rangit river (Vezzoli et al., 2017). Garzanti et al. (2004), Chakraborty and Ghosh (2010), Ghosh (2015), Khan and Islam (2015), have studied the geomorphic, depositional environment and hydrologic characteristics of the Tista fan in the up-stream (Indian section). The mineralogical studies of sediments suggested that Tista sediment in Sikkim is composed mostly of quartz, feldspars and high-grade metamorphic rock fragments from the Greater Himalayan Sequence (GHS), while Rangit sediment is enriched in low-grade metamorphic grains deriving from the Daling successions of the Lesser Himalaya Sequence (LHS) sourced from a glacier of Mt. Kabru in the southern Kangchendzonga region (West Sikkim). Due to the major contribution of Rangit river sediments in the Tista main channel, downstream sediments carry quartz-rich sand, feldspars and low-rank metamorphic lithic grains.

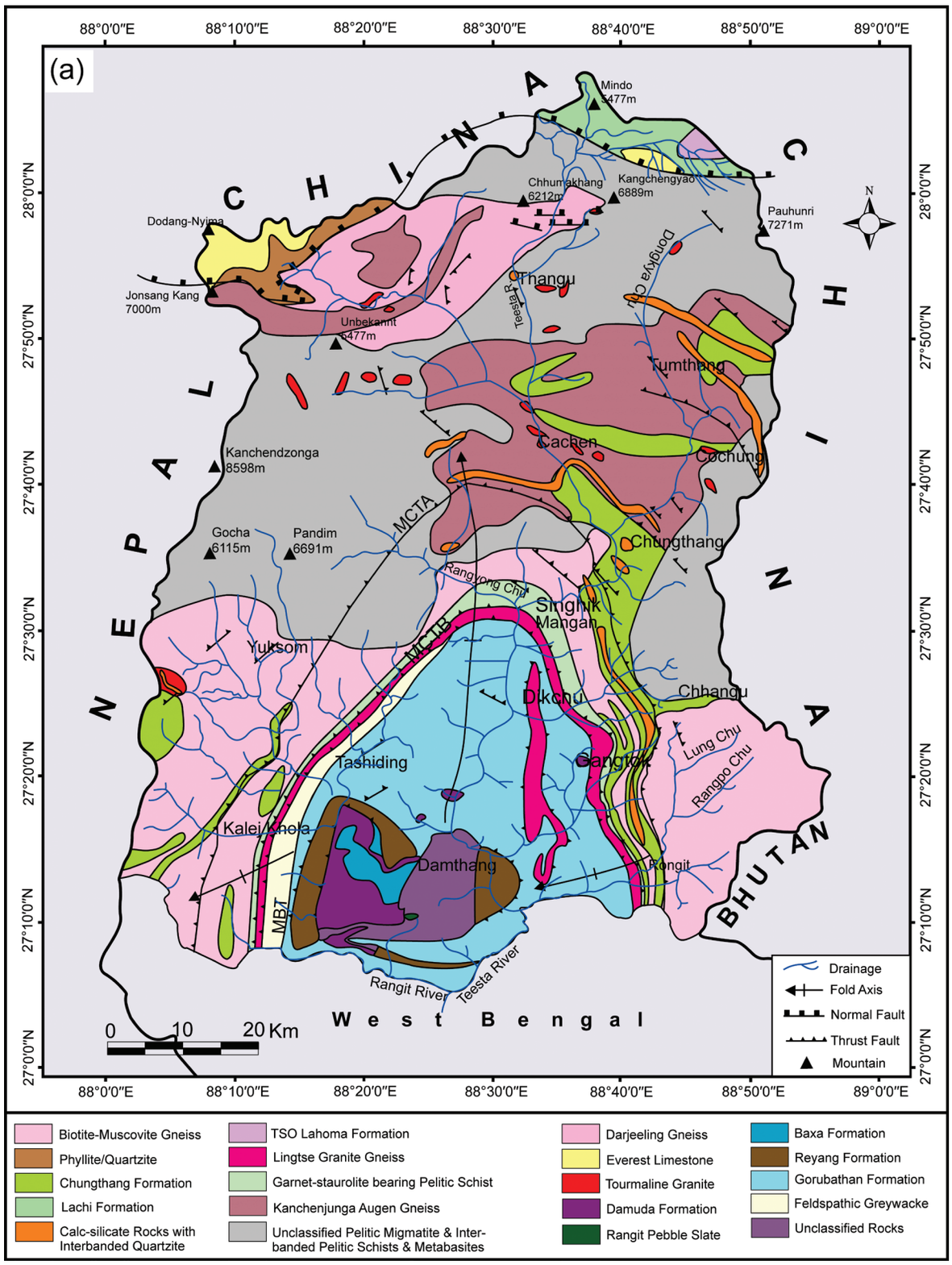

Fig. 1(a): Geological map of Sikkim and Dzongri area indicating catchment area of the Tista river system (modified after Das, 2015).

Several authors studied lower Tista river sediments, among them Ramesh et al. (2000) analysed rare earth elements (REE) and trace elements distribution in surficial sediments. Thereafter, Hossain et al. (2013) focused on glass sand potentiality, and Rahman et al. (2017) introduced techno-economic viability of the river deposits. Biswas et al. (2018) also demonstrated heavy mineral potentiality. However, none of them depicts the provenance type depending on detail geochemical analysis of the Tista river sediments in Bangladesh, which will provide information about the source of minerals for further research applied in the placer mining industry. So, it is necessary to explore the petrography and geochemistry of the Tista fluvial

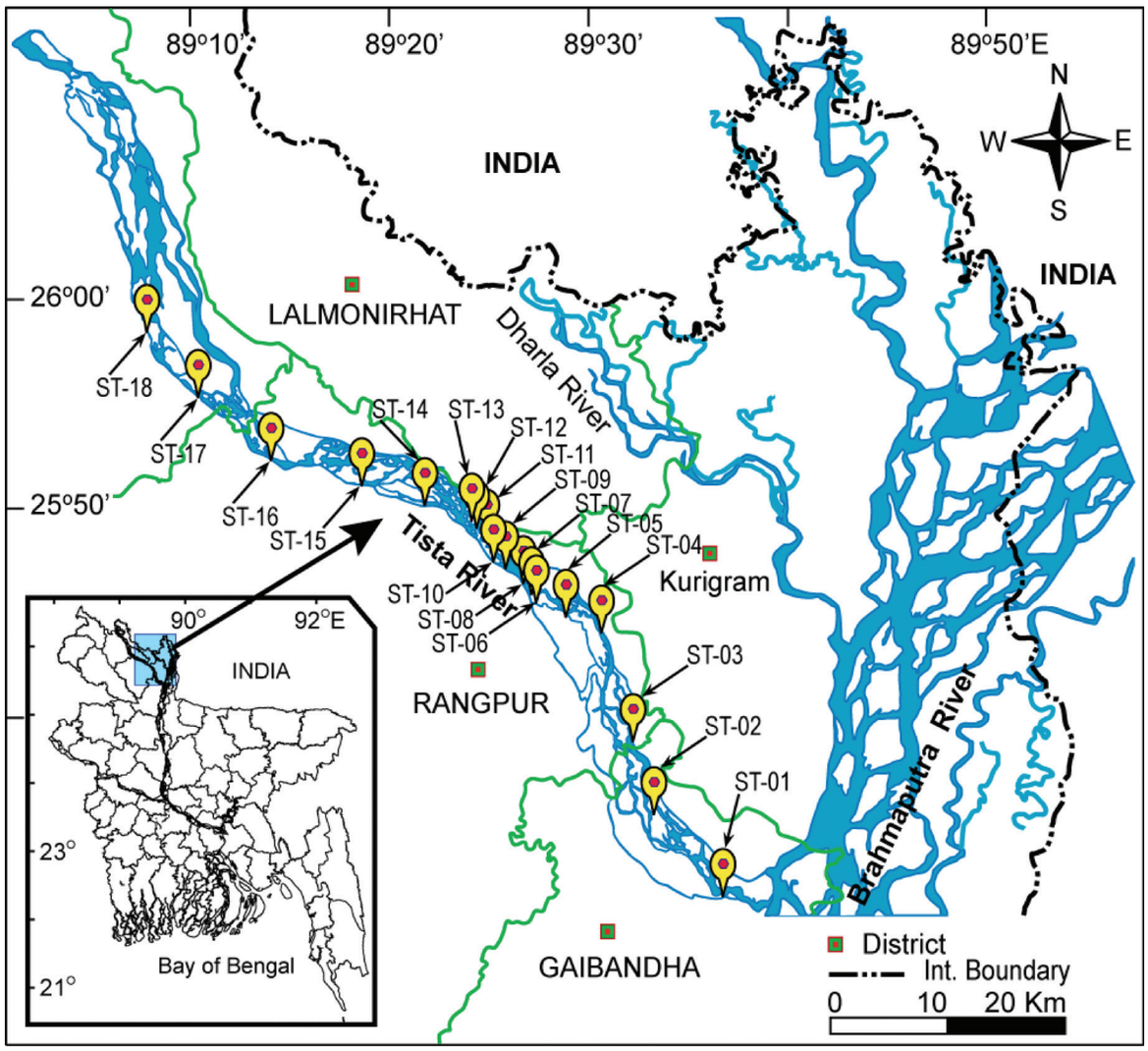

Fig. 1(b): A generalised map showing the study area and sample locations (ST01-ST18) along the Tista river course.

sediments for provenance, tectonics and weathering implications.

GEOLOGY AND GEOMORPHOLOGIC SETTING

Southern Sikkim and Darjeeling Hills are collectively known as the Sikkim Himalaya. The Main Central Thrust (MCT) separates the overlying Greater Himalayan Sequence (GHS) from the Lesser Himalayan Sequence (LHS) (Fig. 1a). The sequence of GH is composed of high grade meta-sedimentaries (e.g., calc-granulities, schist, quartzite), gneisses, migmatites and a number of granitic intrusions in the axial zone of north Sikkim (Mottram et al., 2014). On the other hand, Tista basin in Sikkim is characterized by the LHS unit possesses three distinct supracrustal formations (Fig. 1a): the Palaeoproterozoic Daling Formation the Neoproterozoic-Cambrian Buxa Formation and the much younger Permian Gondwana sediments (Mottram et al., 2014). Further south, the Gondwana sediments are separated tectonically from the Siwalik by the Main Boundary Thrust (MBT) (Fig. 1a).

The Tista river passes through the Darjeeling ridge in a narrow and deep gorge with a meandering course where the elevation ranges from 610 to 747 m, and follows for approximately 160 km. Thereafter it enters Bangladesh at the Kharibari border, Nilphamari district, and joins the Brahamaputra river at Chilmari Thana (Mukhopadhya, 1982). The catchment area, amounting to ~23,300 km^2 (in total) for plains and mountainous area spreads almost all of Sikim, Darjeeling district of India and the northern part of Bangladesh (Hanif, 1995).

MATERIAL AND METHODS

Bulk samples were collected from the surface up to ~1.5 m depth on the riverbanks and chars of the Tista river. All together, 18 samples (labelled as ST) were collected along the river course that covers ~80 km (Table 1, Fig. 1b). Samples were treated with 1N HCl and washed with distilled water to remove organic components. Petrographic analysis was conducted using polished samples following the ribbon method as described in Mange and Maurer (1992).

The geochemical analyses were carried out at the Institute of Mining, Mineralogy and Metallurgy, Joypurhat, Bangladesh following the procedures of Goto and Tatsumi (1994, 1996). A Rigaku ZSX Primus WDXRF machine equipped with an end window 4 kW Rh-anode X-ray tube was used. For the analysis, 32 mm fused beads were prepared by mixing a finely powdered (<75µm) sample with a flux (lithium tetraborate) in a flux/sample ratio of 10:1 and then heated to 900^0C-1000^0C in a platinum crucible and cast into a mold with a flat bottom. The heavy and light elements were determined using 40 kV voltage with 60 mA current respectively. The standards used in the analyses were the Japanese Stream Sediments (JSD 1, JSD 2 and JSD 3). Analytical uncertainties for XRF major and minor elements are ~2% and trace elements are <10%.

In order to examine geochemical behavior of major oxides, weathering pattern of source materials and its control on physical parameters (e.g., grain-size), we performed a principal component analysis (PCA) on geochemical data by using XLSTAT software. The method of MFW (Mafic-Felsic-Weathering) ternary diagram was accomplished as postulated by Ohta and Arai (2007); mentioning, weathering index W* was obtained as calculated W value.

RESULTS

Petrography

The mean grain size (Mz) ranges from 125 to 500 µm with 83 wt% of all materials, 33 and 50 wt% for 250 to 500 µm fraction and 125 to 250 µm fraction, respectively, indicating that the sand grains are medium to coarse in size (Blott and Pye, 2012). The data set of the modal analysis is documented in table 1. The minerals identified in the channel bar and recent deposits on the river bank comprise mostly of quartz, feldspars and mica. Some heavy minerals like magnetite, ilmenite, rutile, zircon, garnet, monazite, kyanite and sillimenite are also present (Biswas et al., 2018) that resemble dominantly sub-angular to sub-round in shape, and moderately mature in texture. Quartz is the main constituent mineral, amounting to 70% of the total volume in which monocrystalline grains are abundant, whereas feldspar and lithic fragments are about 8% and 3%, respectively (Table 1). Lithic fragments are composed mainly of sedimentary and lower-grade metasedimentary (Lms) lithic grains (Vezzoli et al., 2017), which presumably the result of recycling sediment en route traverse through the mainstem.

Geochemistry

Major element concentration

The concentration of major elements found in the bar sand samples of the Tista river bed is presented in table 2. Generally, major element distribution patterns replicate the mineralogy of the studied samples. The sand samples have higher SiO_2 contents and lower Al_2O_3 than the fine-grained mud enriched samples. The

Table 1: Mineralogy of the Tista river sediments in the study area.

Sample	Latitude	Longitude	Quartz	Feldspar	Lithic	Mica	Heavy Minerals	Others
ST-01	25.5510	89.6088	68.23	10.06	3.06	6.45	0.73	11.47
ST-02	25.6165	89.5528	68.40	7.64	3.84	7.74	1.37	11.01
ST-03	25.6716	89.5350	68.37	6.98	4.30	7.26	4.07	9.02
ST-04	25.7528	89.5081	71.29	7.24	3.74	6.48	2.24	9.01
ST-05	25.7628	89.4782	70.05	8.26	3.49	6.50	0.85	10.86
ST-06	25.7761	89.4527	69.93	7.66	3.67	5.90	2.96	9.88
ST-07	25.7814	89.4500	72.08	7.90	2.79	5.81	1.22	10.20
ST-08	25.7923	89.4429	69.18	7.63	3.35	6.69	2.90	10.25
ST-09	25.7973	89.4273	70.30	7.60	3.42	6.13	3.56	8.99
ST-10	25.8048	89.4178	72.73	7.29	3.50	6.77	1.44	8.28
ST-11	25.8164	89.4135	71.64	7.23	3.51	7.19	1.80	8.63
ST-12	25.8240	89.4132	68.50	9.53	3.38	6.22	1.50	10.87
ST-13	25.8393	89.3995	68.28	8.42	3.78	6.44	3.40	9.68
ST-14	25.8481	89.3596	68.33	8.48	3.36	6.54	3.07	10.23
ST-15	25.8614	89.3071	72.24	8.35	2.56	4.89	2.11	9.86
ST-16	25.8795	89.2309	70.07	8.75	3.05	4.81	2.29	11.03
ST-17	25.9230	89.1689	68.68	8.58	3.82	5.99	2.20	10.73
ST-18	25.9766	89.1243	69.25	7.49	4.62	7.52	2.42	8.70

overall chemical compositions of the sediments with respect to sampling locations do not vary widely; SiO_2 from 65.2 to 75.2 wt% with an average of 71.9 wt% and Al_2O_3 from 7.3 wt% to 11.9 wt% with an average of 9.5 wt% (Table 2). The higher percentage of SiO_2 is due to its high quartz contents. The samples are also characterized by relatively high contents of Fe_2O_3 (3.1–9.3 wt%), MgO (1.3–2.6 wt%) and TiO_2 (0.2–1.8 wt%) due to its mafic components, which in turn give off a reflection of significant Ti-bearing minerals e.g., ilmenite, titanite and titaniferous magnetite, biotite in the analyzed samples (Armstrong-Altrin et al., 2004). The content of CaO (avg. 1.4 wt%) indicates that the samples have either carbonate constituent or calcic minerals e.g plagioclase feldspar, garnet. The strong negative correlation (r = -0.8) between SiO_2 to CaO (Table 3) shows that carbonate in all samples preserved, in detrital/matrix form, are primary, since the existence of secondary carbonate could illustrate SiO_2-CaO scatter (Feng and Kerrich, 1990). Most of the samples have lower content of P_2O_5 (avg. 0.13 wt%) compared to UCC (Taylor and McLennan, 1985), which explains the minor number of accessory phases such as apatite and monazite.

Comparing with the values of continentally derived sediments documented by Taylor and McLennan (1985) as Upper Continental Crust (UCC) and post Archean Australian Average Shale (PAAS), SiO_2 is higher in the studied samples (Table 2). Most of the major oxides (e.g., MgO, TiO_2 and Fe_2O_3) have a strong linear negative trend with SiO_2 (Table 3), suggesting that the contents of unstable components in the sedimentary rocks gradually decrease as the maturity of clastic rocks increases by the action of hydraulic fractionation (Singh, 2010). This is evident from Biswas et al. (2018), that finer particles are higher in downstream compared to upstream in the Tista river sands. High correlation coefficients between Fe_2O_3* and TiO_2 (0.97), Fe_2O_3* and MgO (0.75), Fe_2O_3* and MnO (0.96), and TiO_2 and MgO (0.75) as shown in table 3 reveal that these oxides possibly exist in similar mineral phases, specifically biotite, muscovite and garnet. Similarly, in the studied samples TiO_2, Fe_2O_3, MgO, CaO, P_2O_5 and Na_2O show positive correlations with Al_2O_3, while no particular trend is found with MgO, CaO and Na_2O (Table 3). The strong positive correlation of these major oxides with Al_2O_3 and negative correlation to K_2O indicate the absence of illitic clays (Madukwe et al., 2016) and the existence of garnet and micaceous minerals. Na_2O illustrates scattered distribution due to be outlier of a few data (Table 3). A poor correlation of Na_2O and K_2O with SiO_2 suggests minor amount of sodic- and/or potash-feldspars, but may have calcic plagioclase assuming for high CaO in the sediments (Singh, 2009). Again, there is a strong correlation of TiO_2 with Fe_2O_3, MgO, MnO, CaO and P_2O_5 which recommends the composition of sediment is a weathering and recycling product of alkali-basalt source (Negendank et al., 1985). Also, there is a significant correlation between the MnO to MgO and TiO_2 to Fe_2O_3 (Table 3), suggesting a noticeable influence of mafic sources.

Trace element concentrations

Trace element concentrations of the river sediments are reported in table 4. The contents of transition elements e.g., Cr, Co, Ni and Sc shows a wide range from 541.0 to 1829.8 ppm, 6.2 to 40.4 ppm, 2.6 to 26.7 ppm, 11.4 to 46.0 ppm respectively. Table 4 shows SiO_2 has a strong negative correlation with V, Sc, Zr and Co. Again, a comparison between the average content of transition elements and the UCC standard values represents that Tista river sediments are strongly enriched in Cr, Co, Ni and Sc (Table 3; Fig. 2a). The results reflect the paradigm of sorting in particles occurred in transportation which might have caused preferential enrichment of certain minerals possessing homogeneous grain-size fractions (Whitemore et al., 2004), thus the source rocks are evolved with mafic origin (Long et al., 2012). Co and Sc abundances with reduction of SiO_2, and also substantial positive correlations with V and Al_2O_3 (Table 3), suggest Co and Sc are partly controlled by accessory non-aluminous silicate minerals (Rahman and Suzuki, 2007). As opposed to the typical concentrations of large ion lithophile elements (LILE; valency<2) like Rb (avg. 93 ppm), Ba (avg. 386 ppm), Sr (avg. 146.4 ppm) and high field strength elements (HFSE; valency>2) resembling Y (avg. 15 ppm), Zr (avg. 149.2 ppm), Hf (avg. 3.3 ppm), Nb (avg. 14.7 ppm), La (avg. 14.7 ppm) and U (avg. 1.6 ppm) of the sediments are comparatively lower than average UCC values (Taylor and McLennan, 1985), exclusive of Th (avg. 15.5 ppm) and Cs (avg. 5.2 ppm) (Table 4). Noteworthy, comparing mafic rocks, HFSE elements are enriched in felsic rocks (Long et al., 2012), thus geochemical behavior of HFSE suggests the samples are the result of mafic source. Comparing UCC and PAAS, low enrichment of Th may indicate the existence of allanite-monazite, which have to control on REE, e.g., La (avg. 14.7 ppm), Y (avg. 15 ppm) and Gd (4.1 ppm) (Condie et al., 1992). However, poor concentration of Th, P_2O_5, Zr and Y suggest that Th is not controlled mostly by a single mineral (e.g., zircon, clays, apatite or monazite), but more likely by a combination of minerals (Condie, 1991). HFSE, in general, occurs in accessory minerals like rutile and zircon. The samples are relatively depleted in Zr, Hf and Nb (Table 4; Fig. 2a), but unlike Nb, Zr has good correlations with Hf. Thus, it can be inferred, accessory mineral contents are relatively low in Tista river sediments (Long et al., 2012). However, the relation

Table 2: Major element concentrations (wt%) of bar sediments in the Tista river in the northwestern part of Bangladesh.

Oxides	ST-01	ST-02	ST-03	ST-04	ST-05	ST-06	ST-07	ST-08	ST-09	ST-10	ST-11	ST-12	ST-13	ST-14	ST-15	ST-16	ST-17	ST-18	Avg.	UCC[a]	PAAS[a]
SiO_2	72.64	73.45	65.22	74.02	70.68	70.01	72.46	72.19	68.41	71.80	71.11	71.16	74.09	72.61	74.52	75.21	73.27	71.03	71.88	66.00	62.80
Al_2O_3	10.46	11.87	11.72	9.71	9.20	9.15	9.66	7.30	11.70	9.19	9.17	7.51	8.91	8.42	7.89	10.20	9.49	9.96	9.53	15.20	18.90
Fe_2O_3*	3.59	4.00	9.32	3.63	3.94	5.64	3.67	3.57	8.57	4.05	4.27	3.79	3.64	3.98	3.05	3.45	4.09	4.27	4.47	4.50	6.50
MgO	1.54	2.06	2.58	1.54	1.88	2.05	1.35	1.84	2.34	2.06	1.99	2.05	1.41	1.53	1.32	1.38	1.36	2.07	1.80	2.20	2.20
CaO	0.98	1.19	2.42	1.40	1.03	1.31	1.09	1.52	2.43	1.51	1.38	1.47	1.28	1.33	1.11	1.10	1.26	1.34	1.40	4.20	1.30
Na_2O	2.74	2.31	3.07	3.05	2.22	2.04	2.33	2.56	1.71	3.43	3.07	2.34	2.04	2.42	2.29	2.52	2.00	2.57	2.48	3.90	1.20
K_2O	2.91	2.85	1.47	2.19	3.01	2.42	2.61	2.17	1.58	2.36	2.57	2.39	2.13	2.21	2.19	2.29	2.25	2.54	2.34	3.40	3.70
TiO_2	0.35	0.42	1.77	0.39	0.39	0.59	0.40	0.40	1.29	0.48	0.47	0.45	0.32	0.22	0.26	0.31	0.42	0.51	0.52	0.50	1.00
P_2O_5	0.05	0.07	0.40	0.13	0.06	0.11	0.09	0.10	0.40	0.13	0.13	0.12	0.07	0.08	0.06	0.06	0.11	0.12	0.13	0.17	0.16
MnO	0.04	0.05	0.47	0.07	0.05	0.15	0.05	0.08	0.30	0.07	0.06	0.06	0.07	0.07	0.05	0.06	0.07	0.06	0.10		0.11
Total	95.28	98.27	98.44	96.13	92.43	93.49	93.70	91.72	98.73	95.07	94.21	91.33	93.95	92.88	92.73	96.58	94.31	94.48	94.65		
CIA	52.93	57.21	53.78	50.27	51.58	53.06	53.44	44.58	59.46	46.33	47.75	46.01	53.24	49.51	49.63	54.65	55.05	52.15	51.70	47.93	70.38
PIA	54.29	60.26	54.42	50.35	52.49	54.40	55.01	42.41	61.45	45.06	46.83	44.16	54.48	49.32	49.47	56.34	57.05	53.02	52.27	47.31	79.05
CIW	62.95	67.18	58.01	57.29	63.10	62.57	63.34	52.04	65.11	53.19	55.83	54.67	61.76	57.62	58.32	63.03	64.13	60.93	60.06	54.22	82.72
W	26.27	30.56	27.84	22.50	29.79	34.04	28.72	21.55	35.39	21.61	24.25	24.47	26.25	21.35	22.44	25.22	30.78	28.29	26.74	13.12	52.97
ICV	1.16	1.08	1.76	1.26	1.35	1.54	1.18	1.65	1.53	1.51	1.50	1.66	1.21	1.39	1.29	1.08	1.20	1.34	1.37	1.23	0.84
Mn*	0.00	0.01	0.63	0.24	-0.01	0.36	0.08	0.25	0.48	0.14	0.08	0.12	0.23	0.19	0.15	0.20	0.15	0.11	0.19		0.16
Na_2O/K_2O	0.94	0.81	2.09	1.39	0.74	0.84	0.89	1.18	1.08	1.45	1.20	0.98	0.96	1.09	1.05	1.10	0.89	1.01	1.09	1.15	0.32
K_2O/Na_2O	1.06	1.23	0.48	0.72	1.36	1.19	1.12	0.85	0.93	0.69	0.84	1.02	1.05	0.91	0.96	0.91	1.13	0.99	0.97	0.87	3.08
K_2O/Al_2O_3	0.28	0.24	0.13	0.23	0.33	0.26	0.27	0.30	0.13	0.26	0.28	0.32	0.24	0.26	0.28	0.22	0.24	0.26	0.25	0.22	0.20
SiO_2/Al_2O_3	6.95	6.19	5.56	7.62	7.69	7.65	7.50	9.89	5.85	7.81	7.76	9.47	8.31	8.62	9.44	7.37	7.72	7.13	7.70	4.34	3.32
Al_2O_3/SiO_2	0.14	0.16	0.18	0.13	0.13	0.13	0.13	0.10	0.17	0.13	0.13	0.11	0.12	0.12	0.11	0.14	0.13	0.14	0.13	0.23	0.30
Al_2O_3/TiO_2	30.13	28.14	6.62	24.89	23.64	15.59	24.15	18.06	9.05	19.30	19.72	16.66	27.93	38.11	30.35	33.45	22.49	19.52	22.66	30.40	18.90
Fe_2O_3/K_2O	1.23	1.41	6.34	1.66	1.31	2.33	1.41	1.65	5.43	1.71	1.66	1.58	1.71	1.80	1.39	1.50	1.81	1.68	2.09	1.32	1.76
Fe_2O_3+MgO	5.13	6.06	11.90	5.17	5.81	7.69	5.02	5.41	10.91	6.11	6.27	5.84	5.04	5.51	4.37	4.82	5.45	6.33	6.27	6.70	8.70
CaO+Na_2O	3.72	3.50	5.49	4.45	3.25	3.36	3.41	4.08	4.14	4.94	4.45	3.80	3.32	3.75	3.40	3.62	3.25	3.92	3.88	8.10	2.50

Notes: Total iron as Fe_2O_3*; CIA= molar $[Al_2O_3/(Al_2O_3+CaO^*+Na_2O+K_2O)]\times100$; CIW= molar $[Al_2O_3\times100/(Al_2O_3+CaO^*+Na_2O)]$; PIA= molar $[Al_2O_3-K2O)\times100/(Al_2O_3+CaO^*+Na_2O-K_2O)]$; Mn* = $\log[(Mn_{sample}/Mn_{shales})/(Fe_{sample}/Fe_{shales})$; [a]Taylor and McLennan, (1985).

Table 3: Correlation matrix of the Tista river sediments.

	SiO_2	TiO_2	Al_2O_3	Fe_2O_3	MnO	MgO	CaO	Na_2O	K_2O	P_2O_5	Rb	Ba	Sr	V	Cr	Co	Ni	Zr	Sc	Cu	Nb	Zn	La	Ce	Gd	Yb	Y	Hf	Cs	Pb	Th	U	Sb
SiO_2	1																															
TiO_2	-0.88	1																														
Al_2O_3	-0.36	0.59	1																													
Fe_2O_3	-0.88	0.97	0.60	1																												
MnO	-0.83	0.97	0.53	0.96	1																											
MgO	-0.85	0.75	0.40	0.75	0.66	1																										
CaO	-0.78	0.91	0.40	0.90	0.90	0.73	1																									
Na_2O	-0.09	0.06	0.01	-0.07	0.03	0.19	0.05	1																								
K_2O	0.43	-0.68	-0.15	-0.68	-0.77	-0.30	-0.83	0.04	1																							
P_2O_5	-0.82	0.96	0.53	0.95	0.93	0.71	0.97	0.03	-0.78	1																						
Rb	-0.20	0.13	-0.16	0.09	0.07	0.14	0.15	0.23	-0.13	0.16	1																					
Ba	0.18	-0.41	-0.01	-0.41	-0.45	-0.17	-0.64	0.12	0.80	-0.56	-0.21	1																				
Sr	0.91	-0.87	-0.25	-0.90	-0.90	-0.75	-0.86	0.06	0.66	-0.85	-0.05	0.37	1																			
V	-0.90	0.97	0.62	0.99	0.95	0.78	0.89	0.02	-0.63	0.95	0.13	-0.37	-0.88	1																		
Cr	-0.07	-0.04	0.03	-0.02	-0.08	-0.14	-0.18	0.05	0.21	-0.09	0.32	0.24	0.13	0.00	1																	
Co	-0.82	0.95	0.65	0.98	0.97	0.68	0.86	0.00	-0.68	0.92	0.04	-0.37	-0.85	0.97	-0.02	1																
Ni	0.32	-0.12	0.43	-0.21	-0.15	-0.34	-0.28	0.27	0.23	-0.19	-0.05	0.31	0.48	-0.14	0.33	-0.06	1															
Zr	-0.81	0.94	0.51	0.91	0.92	0.65	0.92	0.11	-0.75	0.96	0.26	-0.50	-0.81	0.92	0.05	0.91	-0.01	1														
Sc	-0.80	0.89	0.41	0.91	0.92	0.76	0.91	0.16	-0.76	0.88	0.05	-0.51	-0.88	0.89	-0.14	0.89	-0.33	0.83	1													
Cu	0.26	-0.41	-0.62	-0.49	-0.44	-0.27	-0.32	0.06	0.28	-0.36	0.03	0.13	0.28	-0.46	-0.16	-0.53	-0.14	-0.36	-0.50	1												
Nb	0.11	-0.02	-0.18	0.04	0.06	-0.14	0.23	-0.10	-0.39	0.16	0.06	-0.68	-0.06	-0.01	-0.28	0.03	-0.33	0.12	0.12	0.13	1											
Zn	0.61	-0.38	0.44	-0.38	-0.41	-0.36	-0.43	0.07	0.38	-0.37	-0.25	0.20	0.68	-0.36	-0.14	-0.31	0.57	-0.41	-0.43	-0.18	-0.07	1										
La	-0.09	-0.08	-0.43	-0.12	-0.08	0.06	0.02	0.03	0.05	-0.08	-0.04	0.15	-0.19	-0.12	-0.21	-0.18	-0.29	-0.05	-0.13	0.44	-0.07	-0.36	1									
Ce	0.05	-0.15	-0.39	-0.20	-0.15	0.00	-0.10	0.02	0.13	-0.18	0.01	0.25	-0.06	-0.23	-0.29	-0.27	-0.31	-0.19	-0.18	0.32	-0.13	-0.18	0.89	1								
Gd	-0.17	-0.01	-0.31	-0.06	-0.07	0.21	0.10	0.08	0.09	0.01	0.01	0.12	-0.19	-0.03	-0.07	-0.14	-0.20	0.04	-0.10	0.42	-0.14	-0.32	0.93	0.75	1							
Yb	0.89	-0.78	-0.10	-0.82	-0.78	-0.74	-0.83	0.10	0.61	-0.79	-0.23	0.45	0.94	-0.80	0.09	-0.74	0.56	-0.77	-0.80	0.19	-0.20	0.77	-0.18	-0.01	-0.20	1						
Y	-0.37	0.67	0.64	0.66	0.71	0.23	0.65	0.09	-0.69	0.70	0.14	-0.45	-0.42	0.67	0.03	0.77	0.38	0.79	0.59	-0.49	0.22	0.05	-0.34	-0.41	-0.30	-0.34	1					
Hf	0.93	-0.82	-0.19	-0.85	-0.83	-0.75	-0.77	0.14	0.54	-0.77	-0.12	0.28	0.96	-0.84	0.03	-0.79	0.48	-0.75	-0.80	0.25	0.02	0.76	-0.13	0.01	-0.15	0.95	-0.32	1				
Cs	0.09	0.10	0.21	0.16	0.14	-0.03	0.15	-0.04	-0.27	0.17	-0.10	-0.53	0.03	0.12	0.02	0.17	-0.08	0.07	0.25	-0.17	0.53	0.19	-0.73	-0.69	-0.69	0.00	0.24	0.06	1			
Pb	0.86	-0.74	-0.12	-0.80	-0.71	-0.76	-0.78	0.23	0.51	-0.76	-0.18	0.41	0.89	-0.76	0.03	-0.67	0.67	-0.66	-0.75	0.18	-0.10	0.70	-0.14	-0.03	-0.20	0.93	-0.17	0.91	-0.06	1		
Th	0.87	-0.74	-0.06	-0.74	-0.73	-0.74	-0.67	0.04	0.46	-0.67	-0.31	0.27	0.85	-0.73	-0.11	-0.66	0.52	-0.65	-0.73	0.15	0.08	0.78	-0.06	0.00	-0.09	0.87	-0.16	0.93	-0.02	0.88	1	
U	0.65	-0.67	-0.29	-0.59	-0.57	-0.63	-0.54	-0.01	0.28	-0.59	-0.07	0.19	0.59	-0.58	0.03	-0.46	0.34	-0.48	-0.53	0.09	0.23	0.32	-0.11	-0.16	-0.17	0.49	0.01	0.58	0.00	0.66	0.68	1
Sb	0.30	-0.12	0.18	-0.06	-0.07	-0.23	-0.07	-0.07	-0.10	-0.06	-0.14	-0.35	0.25	-0.10	-0.13	0.00	0.04	-0.11	0.05	-0.31	0.56	0.35	-0.79	-0.66	-0.83	0.18	0.22	0.24	0.81	0.21	0.25	0.30

Table 4: Trace-element concentrations (ppm) of bar sediments in the Tista river in the northwestern part of Bangladesh.

Element	ST-01	ST-02	ST-03	ST-04	ST-05	ST-06	ST-07	ST-08	ST-09	ST-10	ST-11	ST-12	ST-13	ST-14	ST-15	ST-16	ST-17	ST-18	Average	UCC[a]	PAAS[a]
Cu	15.0	11.0	11.0	25.0	27.0	12.0	17.0	22.0	11.0	15.0	16.0	29.0	14.0	16.0	18.0	17.0	18.0	14.0	17.11	25.0	50.0
Co	9.3	12.6	40.4	10.5	9.5	17.2	8.9	6.2	30.5	9.9	11.0	7.5	8.9	14.5	6.4	10.1	10.8	11.5	13.09	10.0	20.0
Ni	22.4	25.4	21.3	18.7	16.0	2.6	20.6	8.8	7.9	17.7	15.4	9.4	15.7	17.5	14.8	22.8	26.7	17.8	16.75	20.0	60.0
Zn	30.6	40.8	14.4	35.1	23.4	20.4	29.3	18.6	24.3	28.6	21.8	15.1	26.9	21.1	22.7	41.6	25.3	31.3	26.18	71.0	85.0
Cr	975.9	835.7	1013.7	640.7	1058.2	1124.9	1269.6	541.0	683.0	1209.7	1490.0	718.8	838.1	942.4	870.4	714.9	1829.8	773.2	973.88	35.0	100.0
Pb	18.1	19.1	6.0	19.6	12.5	7.0	17.1	12.1	1.2	14.3	11.9	9.4	15.2	16.2	17.2	21.2	15.9	14.1	13.77	20.0	20.0
Sr	165.5	171.5	73.0	166.9	140.2	123.8	164.9	134.1	94.8	154.5	147.9	145.3	150.4	143.0	159.9	177.7	169.0	153.2	146.41	350.0	200.0
Th	16.2	16.4	13.3	16.7	15.3	14.1	16.0	15.4	14.7	15.6	15.0	14.4	15.9	16.1	15.6	16.5	15.7	15.6	15.47	10.7	14.6
Sc	14.8	17.2	46.0	19.7	12.3	28.9	11.4	19.3	36.7	26.1	21.3	18.7	21.1	21.0	17.2	15.3	13.4	20.5	21.16	11.0	16.0
V	40.3	47.8	125.8	44.4	48.7	62.7	43.0	36.8	106.2	45.7	58.5	45.0	38.3	47.0	29.9	39.4	44.6	57.2	53.39	60.0	140.0
Zr	129.6	136.2	231.0	140.4	131.1	133.5	150.4	144.1	201.6	150.9	149.6	147.0	130.6	147.8	129.4	134.4	154.5	144.3	149.24	190.0	210.0
Hf	3.4	3.4	3.0	3.5	3.3	3.2	3.4	3.3	3.1	3.4	3.3	3.3	3.4	3.3	3.4	3.5	3.4	3.4	3.35	5.8	5.0
F	636.0	686.0	531.0	454.0	618.0	538.0	482.0	589.0	491.0	544.0	864.0	637.0	541.0	383.0	500.0	637.0	670.0	862.0	592.39		
Sb	3.0	3.0	2.0	3.0	1.0	3.0	3.0	1.0	3.0	3.0	2.0	3.0	3.0	3.0	3.0	3.0	2.0	2.0	2.56		
Ba	439.6	414.3	365.5	370.4	450.1	393.1	382.1	381.9	328.1	379.5	390.6	353.4	350.5	387.4	397.6	372.0	387.8	402.4	385.91	550.0	650.0
Cs	5.0	5.0	5.0	6.0	4.0	6.0	5.0	3.0	6.0	6.0	5.0	6.0	6.0	5.0	5.0	6.0	5.0	4.0	5.17	3.7	6.0
Rb	72.5	57.5	104.0	60.7	51.7	91.0	118.7	107.0	91.0	99.0	146.0	125.0	29.6	88.1	91.0	121.5	117.0	115.0	93.68	112.0	160.0
Nb	14.0	14.0	14.0	16.0	13.0	15.0	16.0	15.0	16.0	15.0	14.0	16.0	15.0	16.0	14.0	15.0	14.0	13.0	14.72	25.0	18.0
Cl	32.0	42.0	42.0	41.0	38.0	38.0	47.0	43.0	38.0	36.0	36.0	39.0	68.0	34.0	33.0	31.0	37.0	40.0	39.72		
U	1.6	1.6	1.3	1.6	1.5	1.4	1.6	1.5	1.4	1.5	1.5	1.5	1.6	2.0	1.6	1.7	1.6	1.6	1.55	2.8	3.1
Y	14.9	15.0	15.1	15.0	14.9	14.9	15.0	14.9	15.0	14.9	14.9	14.9	14.9	15.0	14.9	15.0	15.0	14.9	14.94	22.0	27.0
La	3.0	2.0	13.0	11.0	48.0	2.0	14.0	82.0	7.0	5.0	19.0	9.0	15.0	18.0	1.0	2.0	6.0	8.0	14.72	30.0	38.2
Ce	15.0	13.0	4.0	6.0	42.0	16.0	9.0	104.0	5.0	6.0	16.0	1.0	2.0	1.0	17.0	17.0	1.0	2.0	15.39	64.0	79.6
Gd	3.0	4.0	4.0	4.0	6.0	3.0	4.0	7.0	4.0	4.0	5.0	4.0	4.0	4.0	3.0	3.0	4.0	4.0	4.11	3.8	4.7
Yb	1.6	1.8	0.2	1.8	1.3	0.9	1.4	1.0	0.3	1.4	1.1	0.8	1.4	1.0	1.6	1.8	1.6	1.3	1.24	2.2	2.8
Rb/Sr	0.44	0.34	1.43	0.36	0.37	0.73	0.72	0.80	0.96	0.64	0.99	0.86	0.20	0.62	0.57	0.68	0.69	0.75	0.67	0.32	0.80
Th/U	10.29	10.16	10.20	10.46	10.35	9.81	10.14	10.34	10.69	10.14	9.92	9.62	10.28	8.04	9.81	9.92	9.76	10.08	10.00	3.82	4.71
Th/Sc	1.09	0.95	0.29	0.85	1.24	0.49	1.41	0.80	0.40	0.60	0.70	0.77	0.76	0.76	0.91	1.08	1.17	0.76	0.84	0.97	0.91
Zr/Sc	8.76	7.94	5.02	7.12	10.62	4.62	13.23	7.45	5.50	5.78	7.03	7.85	6.19	7.03	7.52	8.77	11.55	7.02	7.72	17.27	13.13
U/Th	0.10	0.10	0.10	0.10	0.10	0.10	0.10	0.10	0.09	0.10	0.10	0.10	0.10	0.12	0.10	0.10	0.10	0.10	0.10	0.26	0.21
Ni/Co	2.42	2.02	0.53	1.79	1.68	0.15	2.33	1.44	0.26	1.78	1.40	1.25	1.77	1.21	2.30	2.26	2.46	1.55	1.59	2.00	3.00
Cu/Zn	0.49	0.27	0.76	0.71	1.15	0.59	0.58	1.18	0.45	0.53	0.73	1.92	0.52	0.76	0.79	0.41	0.71	0.45	0.72	0.35	0.59
V/Cr	0.04	0.06	0.12	0.07	0.05	0.06	0.03	0.07	0.16	0.04	0.04	0.06	0.05	0.05	0.03	0.06	0.02	0.07	0.06	1.71	1.40
V/Sc	2.73	2.79	2.73	2.25	3.95	2.17	3.78	1.90	2.90	1.75	2.75	2.40	1.82	2.24	1.74	2.57	3.33	2.78	2.59	5.45	8.75
V/(V+Ni)	0.64	0.65	0.86	0.70	0.75	0.96	0.68	0.81	0.93	0.72	0.79	0.83	0.71	0.73	0.67	0.63	0.63	0.76	0.75	0.75	0.70
Cr/Zr	7.53	6.14	4.39	4.56	8.07	8.43	8.44	3.76	3.39	8.01	9.96	4.89	6.42	6.38	6.73	5.32	11.84	5.36	6.64	0.18	0.48

Note: [a]Taylor and McLennan, (1985).

between Zr and Hf signify the presence of zircon, which are not differentiated during weathering and sedimentation processes (Bhatia and Crook, 1986). Again, Nb and Y are not correlated with SiO_2 (Table 3) that proposes weathering, sorting and sedimentation have little impact on them, characterizing sedimentary provenance (Bhatia and Crook, 1986). Likewise, U is not correlated with Al_2O_3 and K_2O (Table 3), suggests clay minerals are not the hosting minerals of the studied samples.

Multi-element normalization

In comparison with the average Upper Continental Crust (Taylor and McLennan, 1985), the studied sediments are depleted in most of the major and trace elements (Fig. 2a). The Multi-element normalized diagram displays enrichment only of SiO_2, Co, Cr, Sc and Th. The largest depletions are seen for CaO, Na_2O, K_2O, P_2O_5, Sr, Pb and Nb at UCC levels (Fig. 2b), indicating a mineralogical (e.g., clays, chlorite, heavy minerals and grain coating) control on sediment geochemistry (Table 1). The experimental result of Na_2O, MnO and CaO is depleted not only due to quartz dilution but also likely due to the sediments have been suffered from intense weathering and recycling (Jin et al., 2006; Tripathia et al., 2007). Fractionation of Sr, strong positive correlation with SiO_2 (Table 3), can be the weathering product of feldspars (mostly plagioclase) due to sorting effects in low temperature depositional environments in the river basin (Rahman and Suzuki, 2007).

Compared with the revised UCC values (Taylor and McLennan, 1985) Siwalik sediments studied by Ranjan and Banerjee (2009) show loss of Ca, Na, Mg, K, P, Sr, Pb, Zr, Nb, Hf and enrichment of Ti, Co, Ni, V, Y, Th (Fig. 2b). Like Brahmaputra-Jumana (Bhuiyan et al., 2011) Tista river shows a consistent result in the enrichment of Th, Cr (very high in Tista), and the depletion of Sr, Pb, Nb, while, Sc and Hf shows disproportionate with each other which may be the resultant of grain size fractionation. Relative to Tista, Brahmaputra river sediments are well-sequestered from inclusion due to their longer traverse way, and eventually sediments become finer (e.g. silt, clay). The geochemical trend of the Tista river sediments is almost consequent to the geochemical behavior of middle (MS) and upper Siwalik (US) sediments. However, Ca and Sr are depleted much faster in lower Siwalik (LS) sediment. Ranjan and Banerjee (2009) reported that these elements (e.g., transition elements, HFSEs and LILEs) get transferred into the clastic sediments during weathering and transportation in the presence of heavy rainfall, and retain the signatures of the parent material like granites and gneisses dominant in the Lesser and Higher Himalayas, respectively.

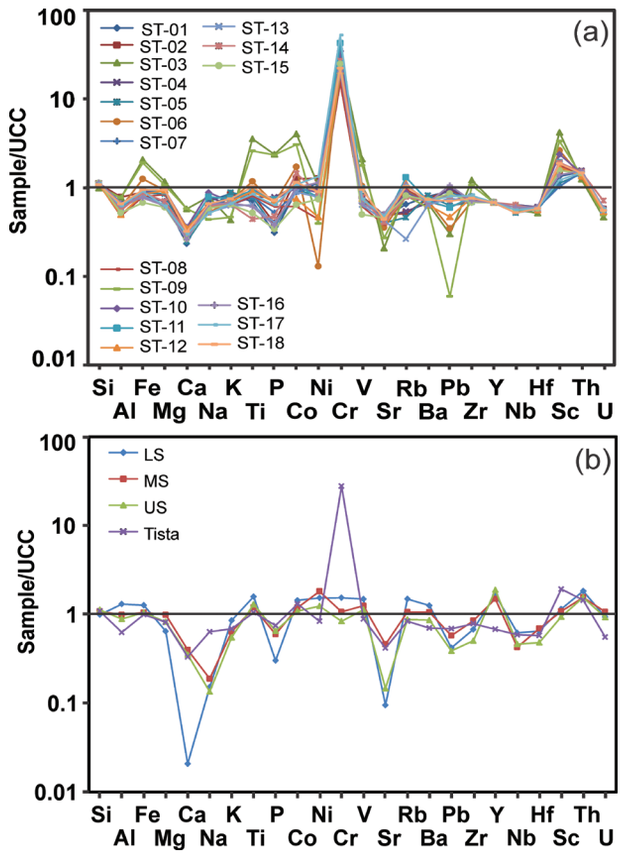

Fig. 2: Multi-element normalized diagrams (a) The data of studied sediments is normalized against UCC (Taylor and McLennan, 1985) (b) A comparison of the normalized value among the Tista river sediments, LS, MS and US sediments (Ranjan and Banerjee, 2009) and Brahmaputra- Jumuna river sediments (Bhuiyan et al., 2011).

DISCUSSION

Geochemical classification and maturity

Many authors have reported a few classification schemes for clastic sedimentary rocks or sediments based on geochemical compositions (e.g., Pettijohn et al., 1972; Crook, 1974; Herron, 1988). According to Pettijohn et al. (1972) and Herron (1988), the chemical composition of the studied samples illustrates dominantly litharenites (Fig. 3a, b). The SiO_2 content and the SiO_2/Al_2O_3 ratio are the most commonly used geochemical criteria for delineating the textural maturity. In general, physical characteristics textural maturity, define as the sorting, matrix content, and angularity of grain in clastic sediments. (Pettijohn, 1975). Potter (1978) and McLennan et al. (1993) documented Textural maturity of sandstones is directly proportionate with SiO_2/Al_2O_3 ratios, whereby increasing ratios of SiO_2/Al_2O_3 for the Tista river sediments vary from 5.56 to 9.89 with an average of 7.70 and are generally higher than that PAAS (3.32) (Table 2), signify textural maturity gradually tend to increase with distance from the source to the burial

depth (Ngama et al., 2019), this resembles the effect of sorting. Variations in the ratios of SiO_2/Al_2O_3 and K_2O/Al_2O_3 may depend on the sediments maturity (Le Maitre 1976; Armstrong-Altrin et al., 2018). Higher SiO_2/Al_2O_3 ratio is observed in litharenites (8.10) than in Fe-sands (5.56), wackes (4.01) and shales (2.31). These ratios increase from fine to coarse sediments in relation to their quartz content.

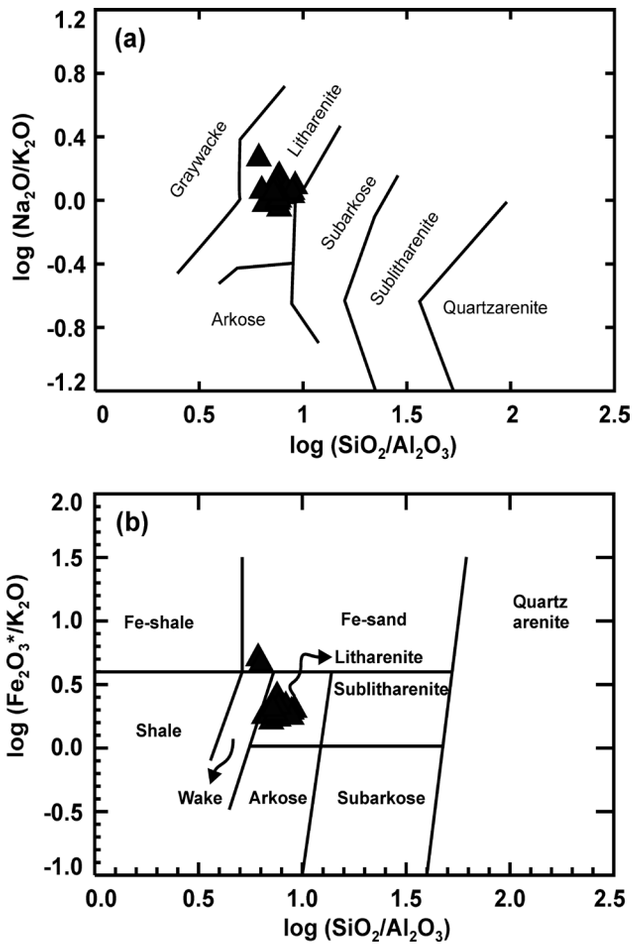

Fig. 3: Geochemical classifications of the Tista river sediments (a) after Pettijohn et al. (1972) and (b) Herron (1988).

Minerals show a relationship between resistances to weathering, which is collectively known as maturity. The Index of Compositional Variability (ICV) is a measure of the compositional maturity of the source material in sedimentary rocks (Cox et al., 1995). ICV is defined as the ratio of the abundance of alumina relative to the other major cations in a rock or mineral, referred to as $(Fe_2O_3 + K_2O + Na_2O + CaO + MgO + MnO + TiO_2)/Al_2O_3$. ICV value in the study area of the Tista river system varies from 1.08 to 1.76 (average 1.37) (Table 2). Major rock forming minerals (e.g., feldspars, amphiboles and pyroxenes) have higher ICV values (>0.84) than clay minerals (<0.84, kaolinite, illite, and muscovite). Noteworthy, lower ICV values indicate recycling and/or high contents of deeply weathered detritus (Cox et al., 1995; Gaillardet et al., 1999). Thus, higher ICV values (>0.84) coupled with lower CIA (Fig. 4) of the studied samples reflect a more immature character and potentially more weak source weathering resulting in sandy nature with immature texture of the source material (Fig. 4).

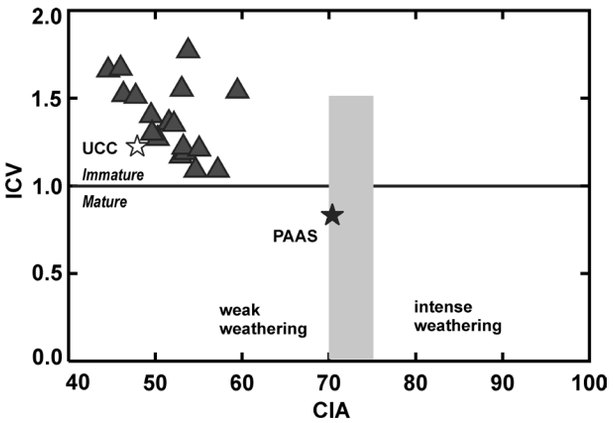

Fig. 4: CIA vs. ICV diagram for the Tista river sediments (after Nesbitt and Young, 1984; Cox et al., 1995). UCC and PAAS data were taken from Taylor and McLennan (1985).

Paleoweathering conditions

The composition of clastic sediments is particularly controlled by the composition of the source rock, duration of weathering, climate and tectonics of the catchment region (Nesbitt and Young, 1982; Wronkiewicz and Condie, 1987). Identification of weathering mechanism, weathering intensity or various chemical weathering indices are useful tools in characterizing and defining the extent of weathering. The enrichment and depletion of alkali and alkaline earth elements (e.g., Ca, Na and K) is presented by the CIA values, since they are largely removed from source rocks during chemical weathering (Nesbitt et al., 1997). Although, the Chemical Index of Alteration (CIA) is a widely used geochemical index to indicate the degree of chemical weathering of the source materials (Nesbitt and Young, 1982; Roy and Roser, 2013), the W* index is very sensitive too (Ohta and Arai, 2007). This index is more significant in order to use more oxides (eight major oxides) than any other conventional indices, thus its applicability extends to a wide range of felsic, intermediate and mafic igneous rock types. Ohta and Arai (2007) introduced a MFW ternary diagram (Fig. 5a), in which M and F vertices define mafic and felsic rock sources in turn, while the W vertex depicts the extent of weathering of these sources, independent of the chemistry of the unweathered parent rock. The W* value increases with an increasing weathering intensity and highly weathered samples plot close to the W vertex. The W* index varies from 21.35 to 35.39 with an average of 26.74 (Table 2) which suggests poor weathering while

the estimated data of the studied sediments fall close to igneous rock trend as similar as unweathered igneous suite like the granodiorite/dacite weathering profile, showing little compositional linear trend extending to the W vertex (Fig. 5a).

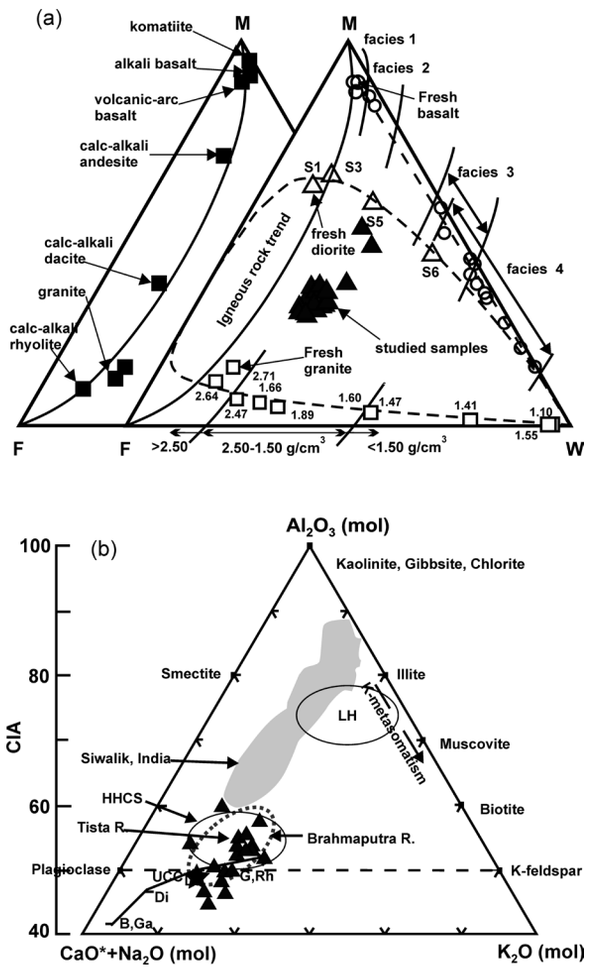

Fig. 5: (a) The MFW ternary plot for the source area weathering of the Tista river sediments. Reference data are plotted for representative igneous rocks by Ohta and Arai (2007) (b) Plots of A-CN-K with CIA values on the vertical axis (after Nesbitt and Young, 1984, 1989) for the Tista river sediments.

On the other hand, CIA values increase with an increasing weathering intensity, reaching 100 for absolutely weathered rocks when all the alkali and alkaline earth elements are leached as weathering residue. In general, the CIA values of average UCC and unaltered granite rocks are approximately 48 and 50 respectively. The CIA value of the samples ranges from 44.6 to 59.5 (average 51.7) (Table 2), which indicates relatively a low degree of chemical weathering in the source area. These results also support by the plagioclase index of alteration (PIA), applicable for the diverse monitoring of plagioclase weathering. The PIA value in unweathered rocks attain 50, while the weathering product of rocks like kaolinite, illite and gibbsite shows 100, in accordance with the estimated values of CIA. In our samples, the PIA values range from 42.4 to 61.5 (avg. 52.3) (Table 2). Likewise, Harnois (1988) proposed Chemical Index of Weathering (CIW), which is almost similar to the CIA. In order to eliminate contribution of K_2O, the calculated result of CIW can reach higher than the CIA, no matter whether the rocks are chemically weathered or not (Fedo et al., 1995). The value of this index increases with the weathering intensity. The CIW values of the studied samples range from 52.0 to 67.2 (average 60.1) which reflects a low intensity of chemical weathering (Table 2). Comparing with the dataset of Holland (1984), the CIW indicates the sediments are the weathering residue of granite (CIW= 60).

On the A-CN-K diagram (Fig. 5b) of Nesbitt and Young (1982), the studied samples plot very close to the plagioclase and K-feldspar tie line, mostly within the Higher Himalayan Crystalline Sequence (HHCS) unit (Singh, 2010) and close to UCC (Taylor and McLennan, 1985) plot proposing very poor weathering conditions where sources are presumably albite-rich with less K mobility. The K_2O/Na_2O ratios (~1) suggest quartz enrichment in the sediments that also reflects by the major elements, especially the high content of SiO_2 (65.2–75.2 wt%) (Table 2). The content of Al_2O_3 (7.3–11.9 wt%), varies significantly that manifests input of feldspar rather than clay minerals existing substantially in the samples. The Rb/Sr ratios of the samples range from 0.20 to 1.43 (avg. 0.67) (Table 4); which is higher than UCC (0.32), while close to PAAS (0.80) (Taylor and McLennan, 1985). Thus, the degree of the source area weathering was most probably poor (Asiedu et al., 2000). The mean CIA value (51.7) of our study sediments is approximately similar to that of the UCC (47.9) and the Ganges river sediments (48–55) in the southwestern Himalayas (Singh, 2010) as well, but they are more similar to those of the Brahmaputra-Jamuna river sediments (51 to 62; avg. 53) (Bhuiyan et al., 2011).

Sorting and sediment recycling

Sorting results in geochemical distinctions among sand, silt and clay due to parting of these grains by hydraulic fractionation and the degree of sorting is controlled by the distance from source to sink, energy of the transport system and many other factors (Roy and Roser, 2012). Gaschnig et al. (2016) reported ICV (>1.5) indicates more mafic (basalt to komatitic) source lithology and ICV (<1.5) represents felsic (granite to granodioritic) composition. Again, Cox et al. (1995) documented, sandstones or shales with ICV (>1) are compositionally immature and were deposited in the tectonically active settings. On the other hand, those with ICV (<1) are compositionally mature and were deposited in a tectonically quiescent or cratonic environment where sediment recycling

was active. The ICV of the sediments is more than 1 (avg. 1.37) as shown in table 2 suggesting that they are fractionation of compositionally immature to moderately mature granite to granodioritic rock and were likely dominated by first cycle input (Cullers and Podkovyrov, 2000).

Garcia et al. (1994) proposed Al_2O_3-TiO_2-Zr ternary diagram which highlights the effects of sorting processes and zircon concentration in sediments. It is noted that shales have higher Al_2O_3/SiO_2 and TiO_2/Zr ratios than their source rocks, whereas sandstones show opposite characteristics in order of maturity of their sources and intensity of sorting processes. Typically, zircons have a strong tendency to be concentrated in the coarse-grained fraction of sediments while TiO_2, although present in heavy minerals such as rutile or ilmenite, is mainly retained in the fine grained alteration products, accompanying with Al_2O_3 (Häussinger and Kukla, 1990). On this ternary diagram (Fig. 6), sediments with a wide range of TiO_2-Zr indicate high compositional maturity, whereas the sediments with a narrow range of TiO_2-Zr variations are compositionally immature. The sediments support a limited range of TiO_2-Zr variation and a clear sorting trend, consisting of sand-size components those are immature, poor to moderately sorted and deposited without recycling.

In sedimentary rocks, Th/U gets particular attention, since weathering and recycling under oxidizing conditions typically result in oxidation of U^{4+} to U^{6+}cause loss of U, leading to an elevation in the Th/U ratio (McLennan et al., 1993). The Th/U and Th/Sc ratios of the studied samples range from 8.0 to 10.7 (avg. 10.0) and 0.29 to 1.41 (avg. 0.84) respectively (Table 4). They summarized geochemical characteristics of provenance types depending on ε_{Nd} (modern sediments), Eu/Eu*, Th/Sc and Th/U, which suggest the river sediments are derivation of rocks formed by much recycling of the old upper continental crust (OUC), the derivatives may resemble high SiO_2/Al_2O_3, CIA, high LILE abundances, uniform compositions. In Fig. 7a, plotting Th/U against Th shows a characteristic feature which is akin to the fine-grained sedimentary rocks (e.g., shale), and indicates normal weathering trend (Taylor and McLennan, 1985; Mbale Ngama et al., 2019). Furthermore, sorting and recycling of sediments can be examined by Th/Sc and Zr/Sc ratios (Kumar et al., 2019). Th/Sc indicates the compositional variation of the source, whereas Zr/Sc ratio is related to zircon enrichments due to sedimentary recycling. On the Th/Sc vs Zr/Sc diagram for clastic sediments, two trends are observed one demonstrates a strong positive correlation between these ratios, while others show a substantial increase in Zr/Sc with far less increase in Th/Sc (Fig. 7b). The first trend can be attributed to the first-cycle sediments if they originated from largely plutonic sources (Rahman and Suzuki, 2007), and can be inferred following the trend consistent with the direct derivation of granitoid rocks (Fig. 7b) (Bhuiyan et al., 2011).

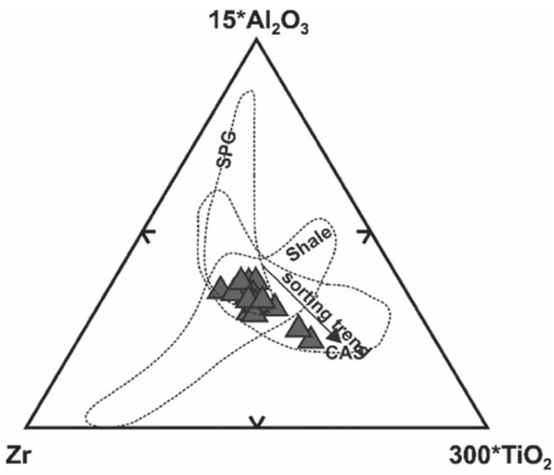

Fig. 6: Ternary plot of 15*Al_2O_3-Zr-300*TiO_2 for the studied sediments. Field of calc-alkaline granites marked as CAS, while field of strongly peraluminous granites denoted as SPG (after Garcia et al., 1994).

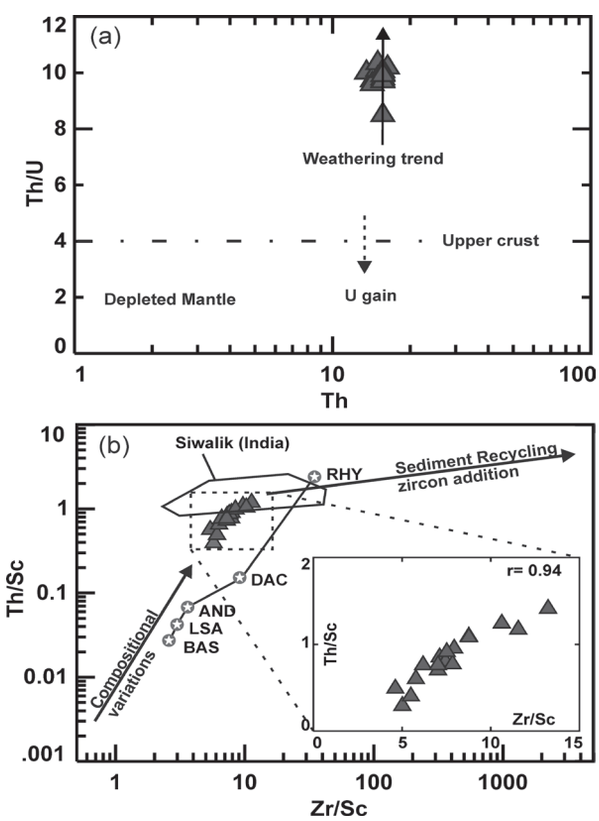

Fig. 7: (a) Th/U vs. Th plot for the Tista river sediments following fields and trends from Gu et al. (2002) (b) Th/Sc–Zr/Sc diagram (McLennan et al., 1993) for the river sediments. Stars: BAS (basalt), LSA (low silica andesite), DAC (dacite) and RHY (rhyolite) as plotted by Roser and Korsch (1999) and Siwalik Group (Ranjan and Banerjee, 2009).

Provenance

Geochemical data in sediments and sedimentary rocks are widely used to assess their provenance signatures as they tend to bear partially the trace of source composition (Taylor and McLennan, 1985; Condie et al., 1992; Keskin, 2011; Garzanti and Resentini, 2016). Dickinson (1985) and McLennan et al. (1993) reported that major elements arrange for evidence on both the rock composition of the provenance and the effects of sedimentary processes like weathering and sorting. The remarkable fact is the proportions of SiO_2/Al_2O_3 (5.6–9.9, avg. 7.7) and K_2O/Na_2O (0.5–1.4, avg. 1.0) of the considered sediments are relatively higher than those proportions of UCC (avg. 4.3 and 0.9 respectively) (Table 2), suggesting the observed sediments were deposited in river a large extent from crustal granitic sources. This result is also consistent with the ratio of Al_2O_3/TiO_2, since the higher ratios (6.6–38.11, avg. 22.7) highlights mostly felsic to intermediate rock sources (Hayashi et al., 1997; Keskin, 2011)

In the discriminant function diagram of Roser and Korsch (1988), all the samples of the present study fall within the quartzose recycled field (P4) (Fig. 8a), which is consistent with a progressive increase in quartz and a decrease in feldspar owing to source weathering and/or sediment recycling (Fig. 10). This consequence is obvious in mature continental provenance where granite-gneiss terrain becomes highly weathered and/or in pre-existing sedimentary or metasedimentary terrain. Published major element datasets from the upper Ganga river and its tributaries in the Himalaya (Singh, 2010) and Siwalik sediments (Ranjan and Banerjee, 2009) were also plotted on the Df1-Df2 diagram (Fig. 8a) for comparison because both rivers Tista and Ganga rise in the GHS unit and traverses over the LHS unit and the Himalayan foreland basin (Siwaliks). The plot of the Ganga river samples falls within the quartzose recycled field (P4) like the studied samples, while major tributaries of Ganga river (such as Bhagirathi river, Mandakini river and Alaknanda river) samples fall within both quartzose (P4) and felsic (P3) field (Fig. 8a). Singh (2010) reported that the resulting composition of the Ganga river sediments is due to the mixing of sediments supplied by these tributaries, where the Bhagirathi and Alaknanda river sediments are dominantly derived from metasediments and those in the Mandakini river from Cambro-Ordovician granites. Thus, the resulting composition of the Tista river sediments was due to the mixing of sediments as described by Singh (2010) for the Ganga river in which mixing and recycled sediments were supplied by its major tributaries.

The studied river sediments contain relatively high concentration of K_2O and Rb, and the value of K/Rb ratios (117–598) lie close to the main trend of K/Rb=230 of a typical differentiated magmatic suite (Fig. 8b) postulated by Shaw (1968). These results highlight compatible nature of the sediments and derivation mainly from acidic to intermediate rocks. Hayashi et al. (1997) stated that the TiO_2/Zr ratios can help to distinguish among three different source rock types, i.e., felsic, intermediate and mafic. The TiO_2 versus Zr plot (Fig. 8c) of the investigated sediments characterize felsic source rocks, which is

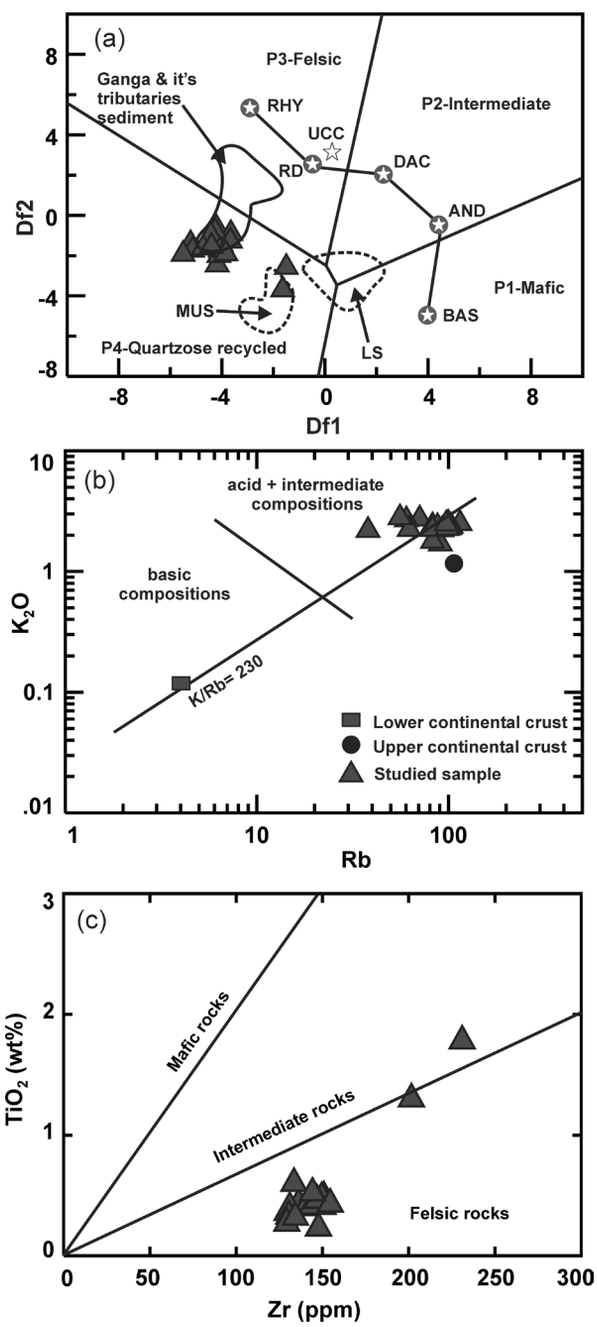

Fig. 8: (a) Major element provenance discriminant plot (Roser and Korsch, 1988) for the Tista river sediments. Stars: BA, AN, DA, RD, RH - average basalt, andesite, dacite, rhyodacite and rhyolite, as plotted by Roser and Korsch (1988) (b) Distribution of K and Rb in the Tista river sediments relative to a K/Rb ratio of 230 (main trend of Shaw, 1968) (c) TiO_2-Zr plot for the studied sediments (Hayashi et al., 1997).

also consistent with the low ratio of TiO_2/Zr (16 to 24), indicating felsic source rocks (Paikaray et al., 2008; Keskin, 2011).

Generally, Cr, Ni, Co and V are useful indicators of mafic and ultramafic source, and they are low in felsic source rocks (Wornkiewicz and Condie, 1987). Nevertheless, presumably some heavy mineral concentrations result in uncertainty in the studied samples, e.g., Cr (541–1829.8 ppm) and Co (6.2–40.4 ppm) concentrations are very high due to the high concentrations of chromian spinel, chromite and magnetite or significant ophiolitic component (Nagarajan et al., 2013). The investigated sediments contain lower concentrations of V (avg. 53.4 ppm), Ba (avg. 385.9 ppm), Sr (avg. 146.4 ppm), Ni (avg. 16.8 ppm), Y (avg. 14.9 ppm) and Zr (avg. 149.2 ppm) than mafic and intermediate source rocks (Table 4) (Taylor and McLennan, 1985; Spalletti et al., 2008). The Cr/Zr ratio is likely to decrease if the concentration of zircons is controlled by hydraulic sorting in the sedimentary process (Taylor and McLennan, 1985; Spalletti et al., 2008). The river sediments show a broad range of Cr/Zr ratios (3.4–11.8) (Table 4), which is identical to the value of the originating from the mafic to felsic sources.

McLennan et al. (1993) extrapolated the relationships of immobile trace elements e.g., Th/Sc–Zr/Sc to evaluate primary source compositions, and also the extent of heavy mineral concentrations arising from recycling or hydraulic sorting. The distribution trend of the studied sediments tends to the oblique right of the primary compositional trend (PCT; Fig. 7b), indicating relative enrichment of zircon. However, the Zr contents range between 129.4–231.0 ppm (Table 4). It is postulated from the petrographic evidence of recycling in the studied sediments (Uddin and Lundberg, 1998), the low ratios of Zr/Sc were produced by simultaneous concentration of labile Sc-bearing phases and zircon. This concentration is supported not only by the strong correlation between Th/Sc–Zr/Sc plotting (Fig. 7b) but also by their strong negative correlation with SiO_2 (Table 3). Thus, the plots of sedimentary trend constrain along the field of the PCT, close to UCC, confirming a felsic source.

Multivariate analysis of major oxides

Principal component analysis (PCA) is a mathematical method of transformation from a large number of variables into a smaller number of independent variables that explain the multivariate data. Eight major elements (variables) dominated source rock composition and weathering, were subjected to clr-transformation and the PCA calculation, as summarized by Ohta and Arai (2007). A factor loading value nearly ±1 demonstrates a strong correlation between the variables and the factor, although the values >± 0.5 are considered significant (Yadav et al., 2018).

The result of PCA of eight major elements dominated source rock composition and weathering of Tista river sediments is given in table 5 and the biplot is demonstrated in figure 9. Compositional variations due to weathering correlate well with PC1, whereas those due to the composition of the unweathered parent rocks correlate with PC2. The variance observed by the variables PC1 is 62.95% and that of PC2 is 14.18% (Table 5). PC1 is, therefore, the prominent variable that controls the geochemical behavior among the studied samples. The cumulative proportions of PC1 and PC2 are 62.95 and 77.13% respectively, representing these two latent variables can explain the majority of the information inherited in the present dataset. The biplot figure shows largely scattered in PC1-PC2 space (Fig. 9a).

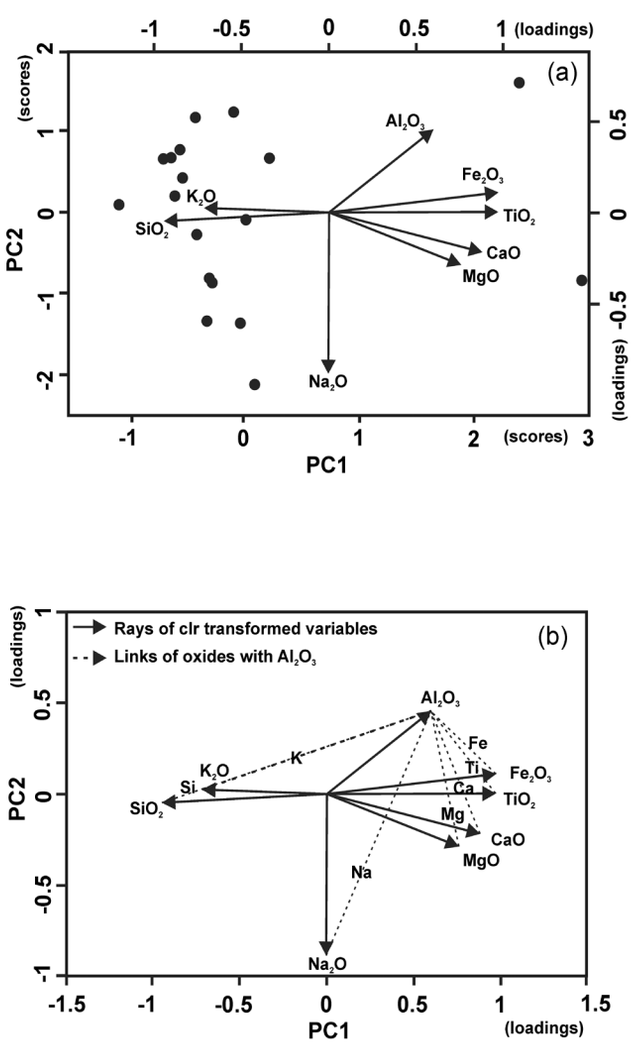

Fig. 9: Relative variation biplot of the clr-transformed data for the Tista river sediments. (a) Scores for samples and loadings of oxides (b) Loadings of oxides and their links. Black dashed arrows indicate links between oxides and Al_2O_3.

Figure 9b displays the loading of each element on PC1 and PC2. The elements that have strong negative loadings with PC1 are SiO_2 (-0.95) and K_2O (-0.72) shows the dominancy of quartz and feldspar (Mongelli et al., 2006; Lim et al., 2013). Also, Na_2O show very weak negative loading (-0.003) and too scattered along PC1 and PC2 to show any affinities with particular elements (Fig. 9b), which represents unweathering signature of parent rocks (Hunger et al., 2018). Samples from each observation are mostly scattered along PC1, indicating the importance of the TiO_2-Fe_2O_3*-MgO-CaO Eigen vector, confirming the effect of heavy-mineral concentration (mostly Fe-Ti-oxides and garnets as placer deposits).

Table 5: Results of principal component analysis.

	PC1	PC2	PC3	PC4	PC5
SiO_2	-0.95	-0.05	0.31	0.00	-0.04
TiO_2	0.97	0.00	0.00	-0.02	0.12
Al_2O_3	0.60	0.45	-0.58	-0.29	-0.13
Fe_2O_3	0.97	0.11	0.05	0.05	0.16
MgO	0.76	-0.29	-0.19	0.48	-0.09
CaO	0.88	-0.22	0.38	0.06	-0.16
Na_2O	0.00	-0.88	-0.35	-0.30	0.02
K_2O	-0.72	0.02	-0.55	0.38	0.04
Eigen value	5.04	1.13	1.04	0.56	0.09
Variability (%)	62.95	14.18	12.98	6.97	1.17
Cumulative (%)	62.95	77.13	90.11	97.07	98.24

Fe_2O_3 and Al_2O_3 are often controlled by particle sizes during transportation and sedimentation in the river system. Both of them concentrate in fine fractions specifically clay minerals (Lim et al., 2013). Noteworthy, in clay minerals or mud rock factor loading in PC1 remain strong positive Al_2O_3 value (Lim et al., 2013; Mongelli et al., 2006). But in our samples, the variable estimated moderate positive loading amounts of 0.60, indicating the studied sediments contain mica, (phyllosilicate minerals). Despite, a positive value of PC1 indicates a contribution from siliciclastic rocks, regardless of mafic or felsic sources.

Tectonic setting

The average Q-F-L ratios (Q_{70}-F_8-L_3) of the analyzed bulk sediments are plotted in the QFL diagram which illustrates no significant variation in the tectonic provenance field at the interim between craton interior and recycled orogeny (Fig. 10) (cf. Dickinson, 1985). Dickinson (1985) has defined this term as deformed and uplifted, dominantly sedimentary strata. In order to have collective effects of weathering and mechanical disintegration, minor differences in the plots may reflect variations in concentrations of quartz relative to feldspar. The studied samples plot close to the Q-F line where the enrichment of quartz, the best indication of felsic source, is privileged dominantly due to the fact of sorting (Fig. 10).

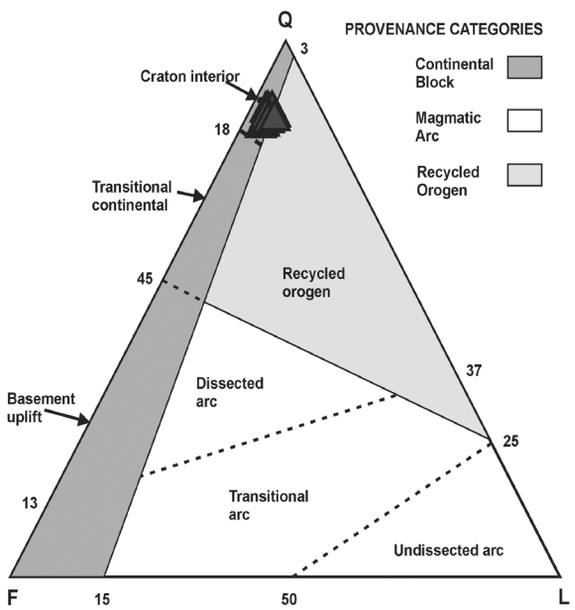

Fig. 10: Quartz-Feldspar-Lithic (QFL) ternary plots of the Tista river sediments after Dickinson (1985).

Clastic sedimentary rocks from different tectonic settings signify varying geochemical characteristics (Bhatia, 1983; Roser and Korsch, 1986). The compatible major and trace-elements are the threshold of various bivariate and multivariate plots inclusive of discrimination functions. These are mostly applicable to the tectonic setting of the sedimentary basins. In the bivariate tectonic discrimination diagram of Roser and Korsch (1986), the plot of studied sediments was in the field of active continental margin (ACM), while one sample was in the field of continental island arc (CIA) (Fig. 11a).

The discrimination function diagram of Bhatia (1983), the plot of DF1 vs. DF2, also demonstrates a consistent result with ACM and a few of the samples bear CIA signatures (Fig. 11b). Based on the oxide composition, Bhatia (1983) suggested a few discrimination diagrams to define tectonic settings. Plots of the samples in the diagrams of (Fe_2O_3+MgO) versus Al_2O_3/SiO_2 fall in the active continental margin field (Fig. 11c). Thus, the river sediments derive from an active continental margin.

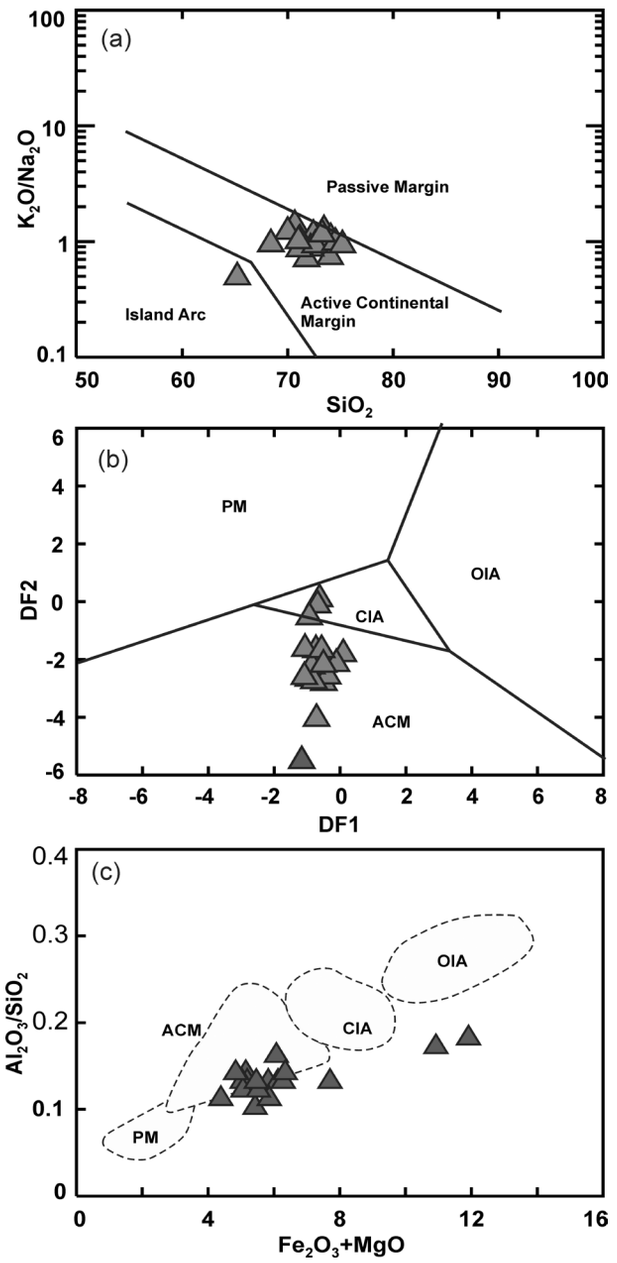

Fig. 11: (a) Tectonic setting discrimination diagram of SiO_2 vs. log (K_2O/Na_2O) for the investigated river sediments (after Roser and Korsch, 1986) (b) and (c) after Bhatia, 1983, where PM= passive margin, ACM= active continental margin, IA= island arc, CIA= continental island arc, OIA= oceanic island arc.

CONCLUSIONS

The bulk geochemistry of recent bar sediments from the Tista river shows wider variations in major elements, reflecting the non-steady-state conditions for provenance, weathering and tectonic setting. Geochemically, the sediments are mainly classified as litharenite. Major, trace elements and their ratios and various discrimination plots suggest that the Tista river sediments are the derivation of an active continental margin which were derived from felsic to intermediate (granitic/Gneiss, quartzite, amphibolite, granulite facies rock type) source rocks, indicating by the enrichment of quartz. The source area may have contained quartzose sedimentary rocks. The sediments deposited in the Tista river resemble those of the Ganges river sediments, exhibit higher SiO_2, Na_2O, K_2O and CaO. High quartz and mafic components give off a reflection of significant Ti-bearing minerals e.g., ilmenite, titanite, titaniferous magnetite and biotite in the analyzed samples. The content of CaO (avg. 1.4 wt%) indicates the samples may have either carbonate constituent or Ca-rich minerals (e.g., garnet, calcic plagioclase). A strong positive correlation between Sr and SiO_2 manifests plagioclase feldspar signature, whereas the strong negative correlation (r= -0.8) between CaO and SiO_2 indicates that carbonate is preserved in all samples, in detrital/matrix form and seems to be primary origin rather than secondary. Strong correlations between TiO_2 to Fe_2O_3, MgO, MnO, CaO and P_2O_5 reflect the source of sediments is mafic dominantly alkali-basalt/greenschist facies. The consistent result is also obvious from HFSE (low value) comparing UCC, the mentioned HFSE elements are enriched in felsic rocks. Among the HFSE the value of Th is higher than UCC, assuming Th is not controlled mostly by a single mineral (e.g., zircon, clays, apatite or monazite), but more likely by a combination of minerals. The values of the weathering indices (W*, CIA, PIA and CIW) along with the elemental ratios indicate that the source rocks supplying the detrital load to the Tista river have not undergone significant chemical weathering. The studied samples are inferred as immature sediments that evidenced from their low SiO_2/Al_2O_3 ratio (7.7), low CIA (51.7) and high ICV (>0.84) values. TiO_2-Zr variation indicates not much mineralogical sorting, which suggests that the sediments are simply the product of mechanically weathered rocks. The geochemical data suggests that the bar sediments of Tista river are the mixture of felsic dominated (e.g., granitic/Gneiss, quartzite, amphibolite, granulite facies rock type) and some parts of mafic source (e.g., alkali-basalt/greenschist facies) and this may happened due to the mixing of sediments supplied by its major tributaries run from Greater Himalayan Sequence (GHS) and Lesser Himalayan Sequence (LHS).

ACKNOWLEDGEMENTS

The authors acknowledge the chairman of BCSIR for funding and all facilities needed in this research. Authors are grateful to Prof. Dr. Ismail Hossain (University of Rajshahi) for his observations and comments in analysing data. Thanks are also extended to Md. Aminur Rahman, Senior Scientific Officer, Md. Sah Alam, Scientific Officers and the staff of IMMM for their cordial support in sampling and data acquisition and anonymous reviewers for their very helpful reviews and constructive suggestions. This

paper is the part of the Ph.D. research work of the first author Pradip Kumar Biswas.

AUTHOR'S CONTRIBUTIONS

P. K. Biswas, M. S. Alam, and S.S. Ahmed proposed the current research as part of the Ph.D. research work of the first author P. K. Biswas. P. K. Biswas and M. N. Zaman conducted field work and sampling. P. K. Biswas and A.S.M. M. Hasan wrote the paper and prepared the figures following acquiesced data. M. S. Alam, S.S. Ahmed, and M.N. Zaman contributed the work with observations and comments in analyzing data and interpretation. All the authors discussed, reviewed and finalized the paper.

REFERENCES

Armstrong-Altrin, J.S., Lee, Y.I., Verma, S.P., Ramasamy, S., 2004, Geochemistry of sandstones from the Upper Miocene Kudankulam Formation, southern India: Implications for provenance, weathering, and tectonic setting. Journal of Sedimentary Research v. 74, pp. 285-297. doi.org/10.1306/082803740285.

Armstrong-Altrin, J.S., Ramos-Vázquez, M.A., Zavala-León, A.C., Montiel-García, P.C., 2018, Provenance discrimination between Atasta and Alvarado beach sands, western Gulf of Mexico, Mexico: Constraints from detrital zircon chemistry and U-Pb geochronology. Geological Journal, v. 53(6), pp. 2824–2848. http://orcid.org/0000-0003-3910-5195.

Asiedu, D.K., Suzuki, S., Nogami, K., Shibata, T., 2000, Geochemistry of Lower Cretaceous sediments, Inner Zone of Southwest Japan: Constraints on provenance and tectonic environment. Geochemical Journal, v. 34, pp. 155-173. doi.org/10.2343/geochemj.34.155.

Bhatia, M.R., Crook, K.A.W., 1986, Trace element characteristics of graywackes and tectonic setting discrimination of sedimentary basin. Contributions to Mineralogy and Petrology, v. 92, pp. 181-193. doi.org/10.1007/BF00375292.

Bhatia, M.R., 1983, Plate tectonics and geochemical composition of sandstones. Journal of Geology, v. 92, pp. 181-193. doi.org/10.1086/628815.

Bhuiyan, M.A.H., Rahman, M.J.J., Dampare, S.B., Suzuki, S., 2011, Provenance, tectonics and source weathering of modern fluvial sediments of the Brahmaputra-Jamuna river, Bangladesh: Inference from geochemistry. Journal of Geochemical Exploration, v. 111, pp. 113-137. doi.org/10.1016/j.gexplo.2011.06.008.

Biswas, P. K., Ahmed, S. S., Pownceby, M. I., Haque, N., Alam, S., Zaman, M. N., & Rahman, M. A., 2018, Heavy mineral resource potential of Tista river sands, Northern Bangladesh, Applied Earth Science, v. 127(3), pp. 94-105. doi.org/10.1080/25726838.2018.1488357

Blott, S.J., Pye, K., 2012, Particle size classes and classification of sediment types based on particle size distributions: review and recommended procedures. Sedimentology, v. 59, pp. 2071-2096. doi.org/10.1111/j.1365-3091.2012.01335.x.

Chakraborty, T., Ghosh, P., 2010, The geomorphology and sedimentology of the Tista megafan, Darjeeling Himalaya: implications for megafan building processes. Geomorphology, v. 115, pp. 252-266. doi.org/10.1016/j.geomorph.2009.06.035.

Condie, K.C., Noll, P.D., Conway, C.M., 1992, Geochemical and detrital mode evidence for two sources of Early Proterozoic metasedimentary rocks from the Tonto Basin Supergroup, central Arizona. Sedimentary Geology, v. 77, pp. 51-76. doi.org/10.1016/0037-0738(92)90103-X.

Condie, K.C., 1991, Another look at rare earth elements in shales. Geochim. Cosmochim. Acta, v. 55, pp. 2521-2531. doi.org/10.1016/0016-7037(91)90370-K.

Cox, R., Low, D.R., Cullers, R.L., 1995, The influence of sediment recycling and basement composition on evolution of mudrock chemistry in the southwestern United States. Geochimica et Cosmochimica Acta 59, 2919-2940. doi.org/10.1016/0016-7037(95)00185-9.

Crook, K.A.W., 1974, Lithogenesis and geotectonics: The significance of compositional variation in flysch arenites (greywackes). Society of Economical, Paleontological and Mineralogical Special Publications, v. 19, pp. 304-310.

Cullers, R.L., Podkovyrov, V.N., 2000, Geochemistry of the Mesoproterozoic Lakhanda shales in southeastern Yakutia, Russia: Implications for mineralogical and provenance control, and recycling. Precambrian Research, v. 104, pp.77-93. doi.org/10.1016/S0301-9268(00)00090-5.

Cullers, R.L., 2000, The geochemistry of shales, siltstones and sandstones of Pennsylvanian-Permian age, Colorado, USA: Implications for provenance and metamorphic studies. Lithos, v. 51, pp. 181-203. doi.org/10.1016/S0024-4937(99)00063-8.

Curray, J.R., Moore, D.G., 1971, Growth of the Bengal deep-sea fan and denudation in the Himalayas. GSA Bulletin, v. 82, pp. 563-572. doi.org/10.1130/0016-7606(1971)82 [563:GOTBDF]2.0.CO;2.

Das, A., 2015, Quaternary Geomorphological Landforms on the Southeast-Facing Slopes of Kanchenjunga around Dzongri in West Sikkim. Ph.D. Thesis (unpublished), available at http://hdl.handle.net/10603/234251.

Dickinson, W.R.,1985, Interpreting Provenance Relations from Detrital Modes of Sandstones. In: Zuffa G.G. (eds) Provenance of Arenites. NATO ASI Series (Series C: Mathematical and Physical Sciences), v. 148. Springer, Dordrecht. https://doi.org/10.1007/978-94-017-2809-6_15

Fedo, C.M., Nesbitt, H.W., Young, G.M., 1995, Unraveling the effects of potassium metasomatism in

sedimentary rock sand paleosols, with implications for paleoweathering conditions and provenance. Geology, v. 23, pp. 921-924. doi.org/10.1130/0091-7613(1995)023<0921:UTEOPM>2.3.CO;2.

Feng, R., Kerrich, R., 1990, Geochemistry of fine-grained clastic sediments in the Archean Abitibi greenstone belt, Canada: implications for provenance and tectonic setting. Geochim. Cosmochim. Acta, v. 54, pp. 1061-1081. doi.org/10.1016/0016-7037(90)90439-R.

Gaillardet, J., Dupré, B., Allègre, C.J., 1999, Geochemistry of large river suspended sediments: silicate weathering or recycling tracer? Geochim. Cosmochim. Acta, v. 63, pp. 4037-4051. doi.org/10.1016/S0016-7037(99)00307-5.

Garcia, D., Fonteilles, M., Moutte, J., 1994, Sedimentary fractionation between Al, Ti, and Zr and genesis of strongly peraluminous granites. Journal of Geology, v. 102, pp. 411-422. doi.org/10.1086/629683.

Garzanti, E., Resentini, A., 2016, Provenance control on chemical indices of weathering (Taiwan river sands). Sediment. Geol., v. 336, pp. 81-95. doi.org/10.1016/j.sedgeo.2015.06.013.

Garzanti, E., Vezzoli, G., Ando, S., Lanord, F.G., Singh, S.K., Fosteret, G., 2004, Sand petrology and focused erosion in collision orogens: the Brahmaputra case. Earth Planet Sc Lett., v. 220, pp. 157-174. doi.org/10.1016/S0012-821X(04)00035-4.

Garzanti, E., Liang, W., Andò, S., Clift, P. D., Resentini, A., Vermeesch, P., Vezzoli, G., 2020, Provenance of Thal Desert sand: Focused erosion in the western Himalayan syntaxis and foreland-basin deposition driven by latest Quaternary climate change, Earth-Science Reviews, https://doi.org/ 10.1016/j.earscirev. 2020. 103220.

Gaschnig, R.M., Rudnick, R.L., McDonough, W.F., Kaufman, A.J., Valley, J.W., Hu, Z., Gao, S., Beck, M.L., 2016, Compositional evolution of the upper continental crust through time, as constrained by ancient glacial diamictites. Geochimica et CosmochimicaActa, v. 186, pp. 316-343. doi.org/10.1016/j.gca.2016.03.020.

Ghosh, K., 2015, Sandy macroforms dynamics and one dimensional facies characterization of the river Teesta. Indian J. Geo. Env. Mang., v.14, pp. 1-15.

Goto, A., Tatsumi Y., 1994, Quantitative analysis of rock samples by an X-ray fluorescence spectrometer (I). The Rigaku Journal, v.11, pp. 40-59.

Goto, A., Tatsumi, Y., 1996, Quantitative analysis of rock samples by an X-ray fluorescence spectrometer (II). The Rigaku Journal, v. 13, pp. 20-38.

Gu, X.X., Liu, J.M., Zheng, M.H., Tang, J.X., Qi, L., 2002, Provenance and Tectonic Setting of the Proterozoic Turbidites in Hunan, South China: Geochemical Evidence. Journal of Sedimentary Research, v. 72 (3), pp. 393-407. doi.org/10.1306/081601720393.

Hanif, S.A., 1995, Hydro-geomorphic characteristics of the Teesta floodplain, Bangladesh. Unpublished Ph.D thesis, Department of Geography, University of Rajshahi.

Harnois, L., 1988, The CIW index- a new chemical index of weathering. Sediment. Geol., v. 55, pp. 319-322. Doi:10.1016/0037-0738(88)90137-6.

Häussinger, H., Kukla, P.A., 1990, The interpretation of geochemical data from metaturbidites using the TiO_2/Zr ratio (abs.): Eur. Jour. Mineral. 2, (n°l, 68 Ann. Meeting of the DGM, Würzburg), 87.

Hayashi, K., Fujisawa, H., Holland, H.D., Ohmoto, H., 1997, Geochemistry of 1.9 Ga sedimentary rocks from northeastern Labrador, Canada. Geochimica et Cosmochimica Acta, v. 61, pp. 4115-4137. doi.org/10.1016/S0016-7037(97)00214-7.

Herron, M.M., 1988, Geochemical classification of terrigeneous sands and shales from core or log data. Journal of Sedimentary Petrology, v. 58, pp. 820-829. doi.org/10.1306/212F8E77-2B24-11D7-8648000102C1865D.

Holland, H.D., 1984, *The Chemical Evolution of the Atmosphere and Oceans.* Princeton University Press, Princeton, N.J. 583 p.

Hossain, I., Ahmed, S.S., Islam, N., Biswas, P.K., Rahman, M.A., 2013, Glass sand potentiality of bar sediments from Tista and Dharla rivers, Bangladesh. Rajshahi University J. Life Earth Agr. Sci., v. 41, pp. 57-64.

Hunger, G., Ventra, D., Moscariello, A., Veiga, G., Chiaradia, M., 2018, High-resolution compositional analysis of a fluvial-fan succession: The Miocene infill of the Cacheuta Basin (central Argentinian foreland). Sedimentary Geology, v. 375, pp. 268-288. doi.org/10.1016/ j.sedgeo.2017.12.004.

Jin, Z., Li, F., Cao, J., Wang, S., Yu, J., 2006, Geochemistry of Daihai Lake sediments, Inner Mongolia, north China: Implications for provenance, sedimentary sorting, and catchment weathering. Geomorphology, v. 80, pp. 147-163. doi.org/10.1016/j.geomorph.2006.02.006.

Keskin, S., 2011, Geochemistry of Çamardı Formation sediments, central Anatolia (Turkey): Implication of source area weathering, provenance, and tectonic setting. Geosciences Journal, v.15, pp. 185-195. doi.org/10.1007/s12303-011-0014-z.

Khan, S.S., Islam, T.A.R., 2015, Anthropogenic impact on morphology of Teesta river in Northern Bangladesh: an exploratory study. J. Geosci. Geomat. v. 3, pp. 50-55.

Kumar, M., Goswami, R., Awasthi, N., Das, R. 2019, Provenance and fate of trace and rare earth elements in the sediment-aquifers systems of Majuli River Island, India. Chemosphere, v. 237, 124477. doi.org/10.1016/j.chemosphere.2019.124477

Le Maitre, R.W., 1976, The chemical variability of some common igneous rocks. J. Petrol., v. 17, pp. 589–637.

Lim, D., Choi, J.Y., Shin, H.H., Rho, K.C., Jung, H.S., 2013, Multielement geochemistry of offshore

sediments in the southeastern Yellow Sea and implications for sediment origin and dispersal. Quaternary International, v. 298, pp. 196-206. doi. org/10.1016/j.quaint.2013. 01.004.

Long, X., Yuan, C., Sun, M., Xiao, W., Wang, Y., Cai, K., Jiang, Y., 2012, Geochemistry and Nd isotopic composition of the Early Paleozoic flysch sequence in the Chinese Altai, Central Asia: evidence for a northward-derived mafic source and insight into model ages in an accretionary orogen. Gondwana Research, v. 22, pp. 554-566. doi.org/10.1016/j. gr.2011. 04.009.

Madukwe, H.Y., Ayodele, S.O., Akinyemi, S.A., Adebayo, O.F., 2016, Classification, maturity, provenance, tectonic setting, and source-area weathering of Ipole and Erin Ijesa stream sediments, south west Nigeria. International Journal of Advanced Scientific and Technical Research, v. 6, pp. 232-255.

Mange, M.A. and Maurer, H.F.W., 1992, *Heavy Minerals in Colour.* Chapman and Hall, London, 147p.

McLennan, S.M., Hemming, S., McDaniel, D.K., Hanson, G.N., 1993, Geochemical approaches to sedimentation, provenance and tectonics. Geological Society of America (Special Paper), 285, pp. 21-40.

Mongelli, G., Critelli, S., Perri, F., Sonnino, M., Perrone, V., 2006, Sedimentary recycling, provenance and paleoweathering from chemistry and mineralogy of Mesozoic continental redbedmudrocks, Peloritani mountains, southern Italy. Geochemical Journal, v. 40(2), pp. 197-209. doi:10.2343/geochemj.40.197.

Mottram, C.M., Argles, T.W., Harris, N.B.W., Parrish, R.R., Horstwood, M.S.A., Warren, C. J., Gupta, S., 2014, Tectonic interleaving along the Main Central Thrust, Sikkim Himalaya. Journal of the Geological Society, London, v. 171, pp. 255-268. doi.org/10.1144/jgs2013-064.

Mukhopadhyay, S.C., 1982, *The Tista Basin: a study of fluvial geomorphology*. In: Bagchi K.P., (ed). The Ganges delta. Calcutta: University of Calcutta Press, 157 p.

Nagarajana, R., Roy, P.D., Jonathan, M.P., Lozano, R., Kessler, F.L., Prasanna, M.V., 2013, Geochemistry of Neogene sedimentary rocks from Borneo Basin, East Malaysia: Paleo-weathering, provenance and tectonic setting. Chemie Der Erde-Geochemistry. doi.org/10.1016/j.chemer.2013.04.003.

Nesbitt, H.W., Young, G.M., 1984, Prediction of some weathering trends of plutonic and volcanic rocks based on thermodynamic and kinetic consideration. Geochimica et CosmochimicaActa, v. 48, pp. 1523-1534. doi.org/10.1016/0016-7037(84)90408-3.

Nesbitt, H.W., Young, G.M., 1989, Formation and diagenesis of weathering profiles. The Journal of Geology, v. 97(2), pp. 129-147. doi.org/10.1086/629290.

Nesbitt, H.W., Young, G.M., 1982, Early Proterozoic climates of sandstone mudstone suites using SiO_2 content and K_2O/Na_2O ratio. Nature, v.299, pp. 715-717.

Nesbitt, H.W., Fedo, C.M., Young, G.G., 1997, Quartz and feldspar stability, steady and non-steady-state weathering, and petrogenesis of siliciclastic sands and muds. Journal of Geology, v. 105, pp. 173-191. doi.org/10.1086/515908.

Negendank, J.F.W., Emmermann, R., Krawczyk, R., Mooser, F., Tobschall, H., Werle, D., 1985, Geological and geochemical investigations on the eastern Trans-Mexican Volcanic Belt. GeofisicaInternacional, v. 24, pp. 477-575.

Ngama, E. M., Sababa, E., Bayiga, E. C., Bessa, A. Z. E., Ndjigui, P. D., & Bilong, P., 2019, Mineralogical and geochemical characterization of the unconsolidated sands from the Mefou River terrace, Yaoundé area, Southern Cameroon. Journal of African Earth Sciences, 159, doi.org/10.1016/j. jafrearsci.2019.103570.

Noa Tang, S.D., Atangana, J.N., Onana, V.L., 2020, Mineralogy and geochemistry of alluvial sediments from the Kadey plain, eastern Cameroon: Implications for provenance, weathering, and tectonic setting, Journal of African Earth Sciences, v.163. doi: https:// doi.org/10.1016/j. jafrearsci.2020.103763

Ohta, T., Arai, H., 2007, Statistical empirical index of chemical weathering in igneous rocks: A new tool for evaluating the degree of weathering. Chemical Geology, v. 240, pp. 280-297. doi.org/10.1016/j. chemgeo.2007.02.017.

Paikaray, S., Banerjee, S., Mukherji, S., 2008, Geochemistry of shales from Paleoproterozoic to NeoprotzoicVindhyan Super-group: Implications on provenance, tectonic and paleoweathering. Journal of Asia Earth Science, v. 32, pp. 34-48.

Pettijohn, F.J., Potter, P.E., Siever, R., 1972, Sand and Sandstone. Plate motions inferred from major element chemistry of lutites. Precambrian Research, v.147, pp. 124-147.

Pettijohn, F.J., 1975, *Sedimentary rocks.* Harper and Row, New York. 491p.

Potter, P.E., 1978, Petrology and chemistry of big river sands. Journal of Geology, v. 86, pp. 423-449. doi. org/10.1086/649711.

Rahman, M.J.J., Suzuki, S., 2007, Geochemistry of sandstones from the Miocene Surma Group, Bengal Basin, Bangladesh: implication for provenance, tectonic setting and weathering. Geochemical Journal, v. 41, pp. 415-428. doi.org/10.2343/ geochemj.41.415.

Rahman, M.A., Zaman, M.N., Biswas, P.K., Sultana, M.S., 2017, Economic Viability of the Tista River Sand Deposits in Bangladesh An Overview. Journal of Scientific Research, v. 9(2), pp. 219-233. doi. org/10.3329/jsr.v9i2.30374.

Ramesh, R., Ramanathan, A. L., Ramesh, S., Purvaja, R., Subramanian, V., 2000, Distribution of rare earth elements and heavy metals in the surficial sediments of the Himalayan river system. Geochemical Journal, v. 34(4), pp. 295-319.

Ranjan, N., Banerjee, D.M., 2009, Central Himalayan crystallines as the primary source for the sandstone-mudstone suites of the Siwalik Group: New geochemical evidence. Gondwana Research, v.16, pp. 687-696. doi.org/10.1016/j.gr.2009.07.005.

Roser, B.P., Korsch, R.J., 1986, Determination of tectonic setting of sandstone mudstone suites using SiO_2 content and K_2O/Na_2O ration. Journal of Geology, v.94, pp. 635-650. doi.org/10.1086/629071.

Roser, B.P., Korsch, R.J., 1988, Provenance signatures of sandstone-mudstone suites determined using discriminant function analysis of major-element data. Chemical Geology, v. 67, pp. 119-139. doi.org/10.1016/0009-2541(88)90010-1.

Roser, B.P., Korsch, R.J., 1999, Geochemical characterization, evolution and source of a Mesozoic accretionary wedge: the Torlesseterrane, New Zealand. Geological Magazine, v. 136(5), pp. 493-512. doi.org/10.1017/S0016756899003003.

Roy, D., Roser, B.P., 2012, Geochemistry of the Tertiary sequence in the Shahbajpur-1 well, Hatia Trough, Bengal Basin, Bangladesh: Provenance, source weathering and province affinity. Journal of Life and Earth Science, v.7, pp.1-13. doi.org/10.3329/jles.v7i0.20115.

Roy, D.K., Roser, B.P., 2013, Climatic control on the composition of Carboniferous-Permian Gondwana sediments, Khalaspir basin, Bangladesh. Gondwana Research, v. 23, pp. 1163–1171. doi.org/10.1016/j.gr.2012.07.006.

Shaw, D.M., 1968, A review of K-Rb fractionation trends by covariance analysis. Geochimica et CosmochimicaActa, v. 32, pp. 573-602. doi.org/10.1016/0016-7037(68)90050-1.

Singh, P., 2010, Geochemistry and provenance of stream sediments of the Ganga river and its major tributaries in the Himalayan region, India. Chem. Geol., v. 269, pp. 220-236. doi.org/10.1016/j.chemgeo.2009.09.020.

Singh, P., 2009, Major, trace and REE geochemistry of the Ganga river sediments: influence of provenance and sedimentary processes. Chem. Geol., v. 266, pp. 251-264. doi.org/10.1016/j. chemgeo.2009.06.013.

Spalletti, L.A., Queralt, I., Matheos, S.D., Colombo, F., Maggi, J., 2008, Sedimentary petrology and geochemistry of siliciclastic rocks from the Upper Jurassic Tordillo Formation (Neuquen Basin, western Argentina): Implications for provenance and tectonic setting. Journal of South American Earth Sciences, v. 25, pp. 440-463.

Taylor, S.R., McLennan, S.M., 1985, *The Continental Crust: Its Composition and Evolution. An Examination of the Geochemical Record Preserved in Sedimentary Rocks.* 312p. Blackwell Science, Oxford.

Tripathia, J.K., Ghazanfari, P., Rajamania, V., Tandon, S.K., 2007, Geochemistry of sediments of the Ganges alluvial plains: evidence of large-scale sediment recycling. Quarter. Int., v.159, pp.119-130. doi.org/10.1016/j.quaint.2006.08.016.

Uddin, A. and Lundberg, N., 1998, Cenozoic history of the Himalayan-Bengal system: Sand composition in the Bengal basin, Bangladesh. Geological Society of America Bulletin, v. 110(4), pp.497-511.

Vezzoli, G., Lombardo, B., Rolfo, F., 2017, Petrology of the Tista and Rangitriver sands (Sikkim, India). Ital. J. Geosci., v. 136, pp. 103-109. doi.org/10.3301/IJG.2016.04.

Whitemore, G.P., Crook, K.A.W., Johnson, D.P., 2004, Grain size control of mineralogy and geochemistry in modern river sediment, New Guinea collision, Papua Guinea. Sediment. Geol., v. 171, pp. 129–157.

Wronkiewicz, D.J., Condie, K.C., 1987, Geochemistry of Archean shales from the Witwatersrand Supergroup, South Africa: Source-area weathering and provenance. Geochimica et CosmochimicaActa, v. 51, pp. 2401-2416. doi.org/10.1016/0016-7037(87)90293-6.

Yadav, K.K., Gupta, N., Kumar, V., Choudhary, P., Khan, S.A., 2018, GIS-based evaluation of groundwater geochemistry and statistical determination of the fate of contaminants in shallow aquifers from different functional areas of Agra city, India: levels and spatial distributions. RSC Advances, v. 8, pp. 15876-15889. DOI: 10.1039/c8ra00577j.